Research Square

Preprints are preliminary reports that have not undergone peer review.
They should not be considered conclusive, used to inform clinical practice,
or referenced by the media as validated information.

Properties of an asphalt binder modified with calcium carbonate micro- and nanoparticles and a reactive elastomeric terpolymer

Conrado Cesar Vitorino Pereira da Silva
Universidade Federal de Campina Grande
Ingridy Minervina Silva
Universidade Federal de Campina Grande
Lêda Christiane de Figueirêdo Lopes Lucena
Universidade Federal de Campina Grande
Sonaly Mendes Arruda
Universidade Federal de Campina Grande
Alexis Jair Enríquez-León
Universidade Federal do Rio de Janeiro
Leni Figueiredo Mathias Leite
Universidade Federal do Rio de Janeiro
Francisco Thiago Sacramento Aragão
fthiago@coc.ufrj.br
Universidade Federal do Rio de Janeiro

Research Article

Keywords: Asphalt binder, calcium carbonate, nanoparticles, reactive elastomeric terpolymer, rheology, fatigue

Posted Date: November 10th, 2026

DOI: https://doi.org/10.21203/rs.3.rs-11468657/v1

License: This work is licensed under a Creative Commons Attribution 4.0 International License.
Read Full License

Additional Declarations: No competing interests reported.

Properties of an asphalt binder modified with calcium carbonate micro- and nanoparticles and a reactive elastomeric terpolymer

Abstract

This study evaluated calcium carbonate ($CaCO_3$) micro- and nanoparticles as modifiers of a penetration-grade asphalt binder (CAP 50/70), alone and combined with 1.8% of a reactive elastomeric terpolymer (RET). Three contents (3%, 7%, and 10%) were compared with the neat binder and a commercial polymer-modified binder (AMP 60/85-E). The fourteen binders were characterised by Fourier transform infrared spectroscopy (FTIR), by empirical tests before and after short-term ageing, and by performance grade, multiple stress creep and recovery, and linear amplitude sweep (LAS). The particles alone produced no qualitative chemical change, whereas combining them with the terpolymer altered FTIR bands and lowered the oxidation indices. Non-recoverable creep compliance at 3.2 kPa fell from 4.4 1/kPa for CAP 50/70 to 0.9 1/kPa with 10% particles and RET, reaching the V traffic designation; within the terpolymer systems, the particles accounted for 0.04 1/kPa per 1% of content. The LAS fatigue ranking changed with the failure criterion: at 1.25% strain, 3% nano-$CaCO_3$ with RET reached 4.5 times the fatigue life of CAP 50/70 under the stored pseudo-strain energy criterion, whereas the 7% system led under the crack-growth criterion. Master curves of the 7% nano- and micro-$CaCO_3$ binders nearly coincided, so the loss of fatigue efficiency at high nanoparticle contents arises in the damage regime, not from a stiffening particle network. Weighting rutting, fatigue, and short-term ageing equally, 7% nano-$CaCO_3$ with RET ranked first, ahead of AMP 60/85-E; the ordering of the binder groups held under ten alternative scoring schemes, whereas the leading position did not.

Keywords: Asphalt binder; calcium carbonate; nanoparticles; reactive elastomeric terpolymer; rheology; fatigue

1. Introduction

Permanent deformation and fatigue cracking are among the main deterioration mechanisms of asphalt surface layers, reducing pavement service life and functional performance. Permanent deformation accumulates as irreversible plastic strain under repeated vehicle loading and intensifies at high temperatures and under heavy traffic, progressively degrading the riding surface (Sun et al., 2016). Fatigue cracking results from repeated cyclic loading, which induces the nucleation of microcracks that propagate and coalesce, producing visible surface cracks and, ultimately, more severe distress (Cheng et al., 2022; Alamnie et al., 2023; Yang et al., 2023; Lu et al., 2024).

Binder modification has been widely adopted to mitigate these damage mechanisms and improve the mechanical performance of asphalt materials (Staub de Melo et al., 2023; Hamedi et al., 2023; Yao et al., 2013; Zhang et al., 2021; Ashish & Singh, 2019). Modification may rely on polymers, mineral fillers, fibres, and, more recently, micro- and nanomaterials, which have shown technical and economic feasibility in paving applications (Anupam et al., 2022). Styrene-butadiene-styrene (SBS), ethylene-vinyl acetate (EVA), and crumb rubber remain the most common modifiers, and SBS alone accounts for more than half of the global modified asphalt market, with projected annual growth of 3% to 4% through 2035 (Business Research Insights, 2024). In Brazil, modified binders are increasingly specified for highways and urban roads subjected to heavy traffic.

Calcium carbonate ($CaCO_3$) micro- and nanoparticles are attractive binder modifiers because of their low production cost, high specific surface area, and consolidated industrial supply as fillers, extenders, and pigments (He et al., 2013; Tsuzuki & McCormick, 2004; Sargheini et al., 2012). Nanomaterials combine low-temperature sensitivity, large specific surface area, and high resistance to permanent deformation (Azahar et al., 2015) and can contribute to more durable pavements with improved resistance to fatigue cracking, thermal cracking, and moisture damage (Santos et al., 2015). The interaction of calcite with the binder is physical and interfacial. Its surface carries a positive potential and a predominantly dispersive surface energy, which favours bonding with the polar fractions of the binder and makes carbonate surfaces lose less adhesion in the presence of water than silicate surfaces (Zhou et al., 2026). In a filler-binder system, a rigid mineral phase stiffens the matrix in proportion to its volume fraction and to the binder layer immobilised at the particle surface, and a continuous particle network, with the plateau in the storage modulus that it imposes at low frequencies, forms only above a critical concentration that depends on the fineness and packing of the filler (Lesueur, 2009). Specific surface area and agglomeration state therefore matter as much as the nominal particle size, and a comparison between micro- and nanoparticles has to be read with those variables in mind.

Reactive polymers are also effective in improving binder performance under heavy traffic and harsh climate conditions. Polimul S74, a reactive elastomeric terpolymer (RET) made of ethylene, methyl acrylate, and glycidyl methacrylate (EMA-GMA), combines elastic behaviour with strong reactivity with the asphalt matrix (Duarte et al., 2023). This interaction helps form a stable polymer network, increasing elasticity and resistance to permanent deformation.

Previous studies have examined these two modifiers separately, and their results do not combine into a prediction for the joint system. Regarding the mineral modifier, Manfro et al. (2022) reported improved resistance to permanent deformation under moisture conditioning in a mixture produced with a binder modified with nano-$CaCO_3$, Albayati et al. (2024) observed increases in binder consistency, rutting resistance, and durability through the combined use of nano-$CaCO_3$ and nano-hydrated lime, and Zhang et al. (2021) obtained a similar stiffening with nano-TiO_2/$CaCO_3$. These studies share two features: they report gains in stiffness-related properties at a single particle size, and they do not examine fatigue beyond the linear viscoelastic range, so they leave open whether the stiffening produced by a rigid filler, which raises the peak stress, also raises the damage tolerance of the binder, and whether nanoparticles do anything that an equal mass of microparticles of the same mineral would not. Regarding the polymer modifier, Gama (2016) and Queiroz (2022) defined the optimum content of the EMA-GMA terpolymer and examined its effects on the rheology of the neat binder, and Duarte et al. (2023) described the reaction between the glycidyl methacrylate group and the asphalt matrix; none of these studies included mineral particles, and none asked whether a mineral phase changes what the terpolymer does. Three research questions therefore remain unresolved: whether particle size, micro or nano, continues to govern binder response in the presence of a reactive polymer; whether particle content continues to influence binder behaviour after polymer incorporation; and whether the combined modification can attain the performance of a commercial high-performance binder across chemical, empirical, and rheological scales, including fatigue response.

This study addresses these questions by evaluating $CaCO_3$ micro- and nanoparticles at 3%, 7%, and 10% by binder mass, both alone and combined with 1.8% RET, in a CAP 50/70 binder benchmarked against AMP 60/85-E. Its contribution lies in a unified experimental programme that relates chemical evidence of particle-polymer-binder interaction to empirical consistency and ageing indicators, as well as to rheological behaviour under permanent deformation and fatigue,

with fatigue assessed under two failure criteria and a set of LAS indices that are seldom reported together for particle-modified binders. The three distresses are then weighed jointly through a composite score whose construction is made explicit and tested for sensitivity, rather than evaluated one at a time. The design compares each particle-modified binder with its terpolymer counterpart, and the contributions of the two modifiers are apportioned from the dependence of each property on the particle content within the terpolymer systems.

2. Materials and methods

This section describes the materials used in this study and the procedures adopted to obtain the chemical, empirical, and rheological properties of the asphalt binders. The tests followed methods from ASTM, the Brazilian Association of Technical Standards (ABNT), the Brazilian National Department of Transport Infrastructure (DNIT), and the American Association of State Highway and Transportation Officials (AASHTO). Fig. 1 presents the flowchart of the experimental programme.

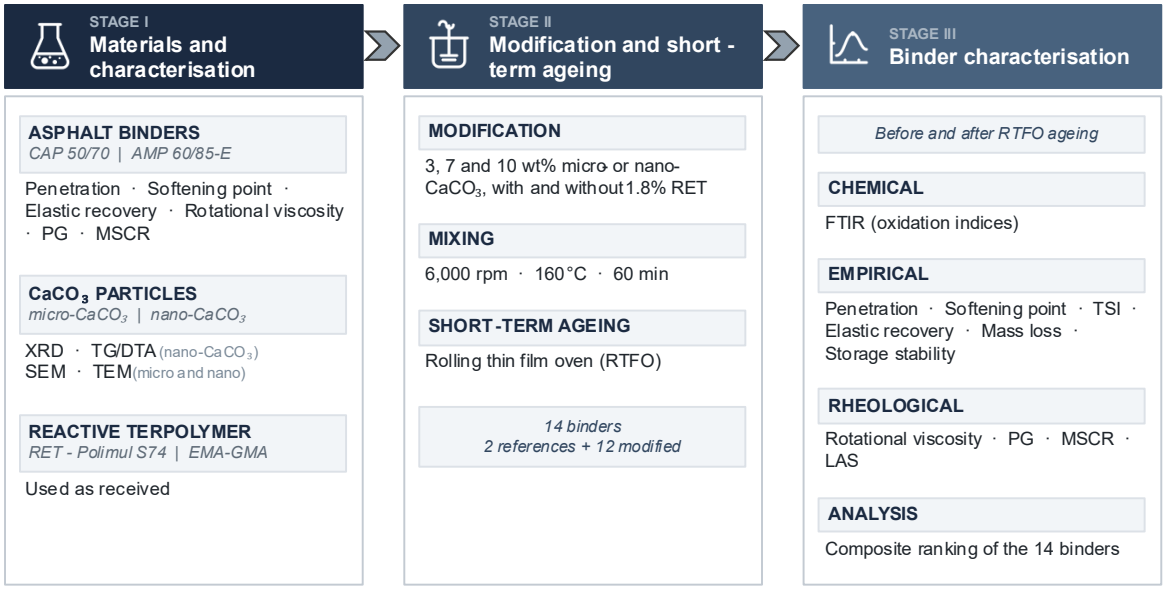


Fig. 1. Flowchart of the experimental programme.

2.1. Materials

2.1.1. Asphalt binders

Two reference binders were adopted for benchmarking. The first was a penetration-graded neat asphalt binder, designated CAP 50/70 in accordance with Brazilian National Agency of Petroleum, Natural Gas and Biofuels (ANP) Resolution No. 897/2022, supplied by Lubnor Petrobras refinery (Maracanaú, CE, Brazil), and selected because of its extensive use in Brazilian flexible pavement structures. The second was a commercial elastomeric polymer-modified asphalt binder, classified as AMP 60/85-E and supplied by Greca Asfaltos, used as the high-performance reference material. Table 1 reports the empirical and rheological characterisation of both binders before and after short-term ageing in the rolling thin-film oven (RTFO), together with the corresponding test standards. The measured properties complied with the specification limits established in DNIT 095/2006-EM and ANP Resolution No. 897/2022, confirming the suitability of the reference binders and their consistency with previous studies that used the same materials (Melo Neto et al., 2020; Sousa Neto et al., 2022).

Table 1. Empirical and rheological characterisation of the reference binders.

Test	Standard	Unit	AMP 60/85-E			CAP 50/70		
			Result	Min	Max	Result	Min	Max
Rotational viscosity, 135 °C	NBR 15184	cP	1060	-	3000	377	274	-
Rotational viscosity, 150 °C	NBR 15184	cP	496	-	2000	188	112	-
Rotational viscosity, 177 °C	NBR 15184	cP	178	-	1000	69	57	285
Penetration, 25 °C, 5 s, 100 g	NBR 6576	0.1 mm	41	40	70	59	50	70
Softening point	NBR 6560	°C	60	60	-	48	46	-
Elastic recovery	NBR 15086	%	86	85	-	-	-	-
Highest PG temperature	ASTM D6373	°C	70	-	-	64	-	-
MSCR $Jnr_{0.1}$	DNIT 423/2020	1/kPa	0.8	-	-	4.2	-	-
MSCR $Jnr_{3.2}$	DNIT 423/2020	1/kPa	1.1	-	-	4.4	-	-
Specific gravity	NBR 6296	g/cm^3	1.05	-	-	1.01	-	-

PG = performance grade; MSCR = multiple stress creep and recovery; Jnr = non-recoverable creep compliance.

The CAP 50/70 used in this research corresponds to the standard traffic designation (S), while the AMP 60/85-E corresponds to heavy traffic (H), according to AASHTO M 332.

2.1.2. $CaCO_3$ micro- and nanoparticles

The $CaCO_3$ micro- and nanoparticles were supplied by Lagos Indústria Química. They were selected because of their lower acquisition cost compared with other nanomaterials and because they are industrial products with a consolidated market and potential for scaled-up production. The two products are the same mineral, sold in two nominal size classes, so the chemical and thermal characterisation by X-ray fluorescence (XRF), X-ray diffraction (XRD), thermogravimetry (TG), and differential thermal analysis (DTA) was performed on the nano-$CaCO_3$ alone, whereas the morphology, particle dimensions, and agglomeration state of both products were examined by scanning electron microscopy (SEM) and transmission electron microscopy (TEM). XRF identified CaO (99.24%), SiO_2 (0.57%), and SrO (0.19%). Fig. 2 presents the XRD pattern of the nano-$CaCO_3$. Diffraction peaks related to impurities were not observed, confirming the purity of the material. The high CaO concentration indicates high $CaCO_3$ content, which favours chemical reactivity, particularly in acid neutralization processes, and can improve the mechanical properties and the thermal stability of composite materials.

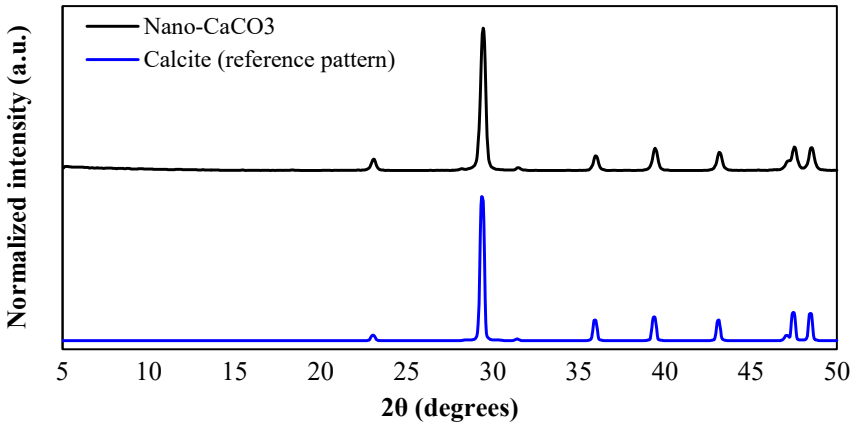
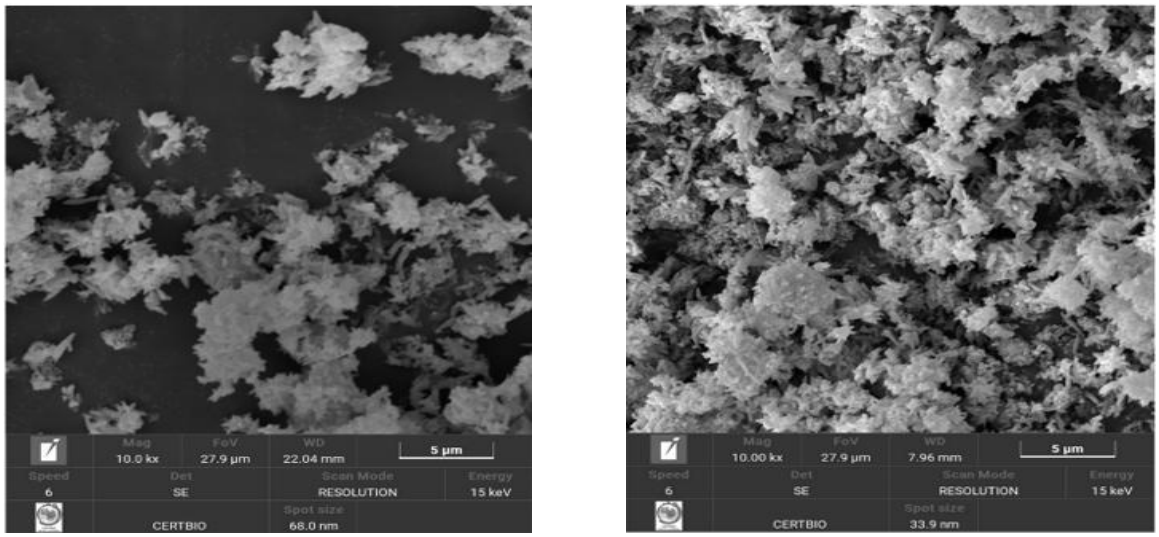


Fig. 2. XRD pattern of the nano-$CaCO_3$.

SEM was used to investigate particle morphology at magnifications from 3,000 to 50,000 times. Fig. 3 shows the micro-$CaCO_3$ (a) and the nano-$CaCO_3$ (b) at a magnification of 10,000 times. Both products appear as agglomerates rather than as isolated particles. The micro-$CaCO_3$ forms compact clusters a few micrometers across, with irregular contours and a rough surface, and the nano-$CaCO_3$ forms finer and more porous agglomerates, with no crystal habit resolvable at this magnification. The agglomeration is consistent with the high surface energy of the particles and is also visible in the TEM images (Fig. 5).



(a) (b)

Fig. 3. SEM images of the micro-$CaCO_3$ (a) and nano-$CaCO_3$ (b).

TG and DTA were used to characterise the thermal behaviour and stability of nano-$CaCO_3$. Fig. 4 presents the remaining mass and the DTA signal as a function of temperature. Two events are resolved. The first is a gradual loss of 4.18% up to about 600 °C, attributed mainly to the release of adsorbed water. The second is a loss of 41.18% between about 600 °C and 800 °C, with an endothermic DTA peak near 780 °C, which corresponds to the decarbonation of $CaCO_3$ into CaO and CO_2; the residual mass of about 55% is close to the stoichiometric CaO yield of 56.0% and corroborates the purity indicated by the XRD pattern. Binder modification, mixing, and compaction occur between 145 °C and 170 °C, far below the onset of decarbonation, so the material does not decompose under processing conditions.

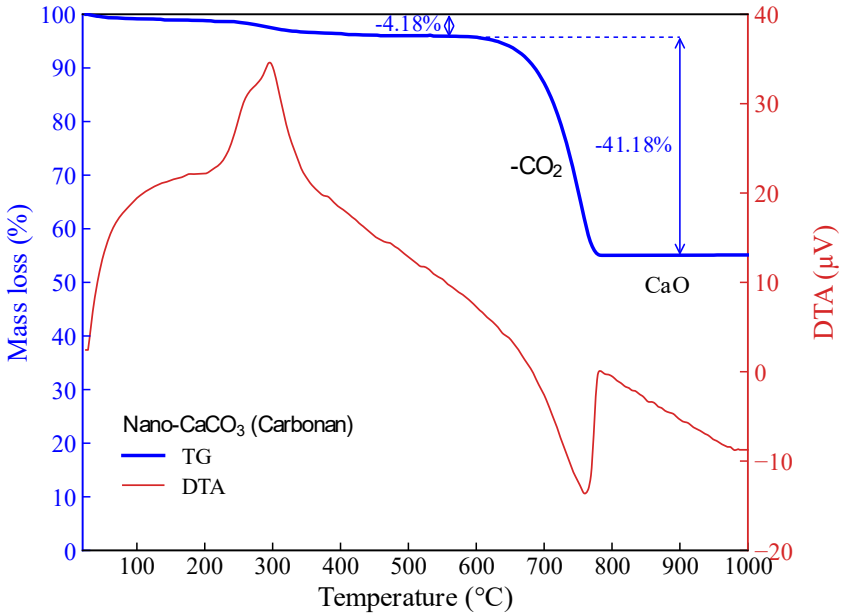
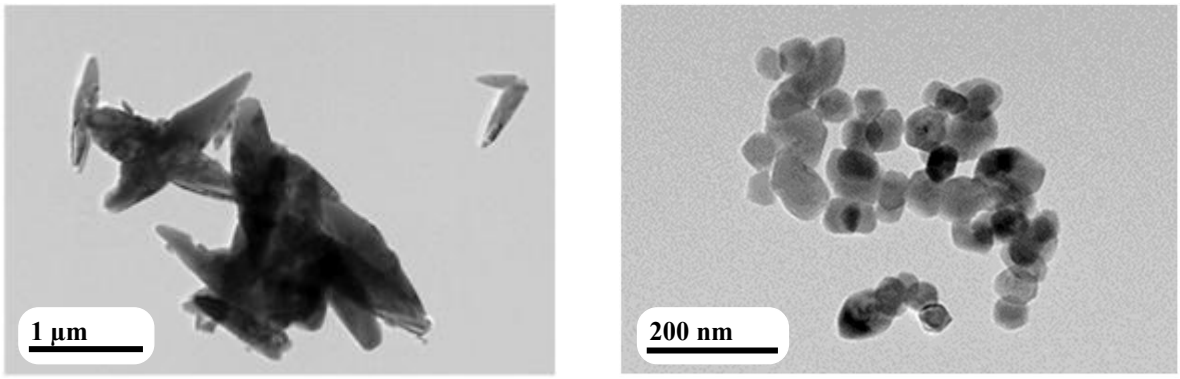


Fig. 4. TG and DTA curves of the nano-$CaCO_3$.

TEM was used to determine the diameter, shape, and structure of the particles, with a JEM-2100 microscope (JEOL Ltd.) operating at 200 kV. Fig. 5 presents the images obtained. The micro-$CaCO_3$ (Fig. 5a) exhibits irregular morphology, with angular contours and overlapping lamellar structures; dimensions range from approximately 0.5 µm to 2 µm, and the contrast variation suggests particle overlap or local thickness variations. The evident agglomeration may originate from the surface affinity of the particles or from sample preparation. The nano-$CaCO_3$ (Fig. 5b) shows predominantly spherical or subspherical morphology, mean diameters below 100 nm, and relatively uniform size distribution, indicating a controlled aqueous synthesis, although with a tendency to agglomerate because of the high surface energy.



(a) (b)

Fig. 5. TEM images of the micro-$CaCO_3$ (a) and nano-$CaCO_3$ (b).

2.1.3. Reactive terpolymer

The reactive elastomeric terpolymer (RET) based on EMA-GMA, with a GMA content of 6% and commercially designated Polimul S74, was supplied by Quimigel. Its selection was motivated by its specific commercial use in paving and by previous research demonstrating its

effectiveness in improving the chemical, physical, and rheological properties of asphalt binders (Gama, 2016; Queiroz, 2022; Duarte et al., 2023). Fig. 6 shows the granules of the terpolymer.



Fig. 6. Granules of the reactive elastomeric terpolymer **(**RET**)** Polimul S74.

2.2. Methods

2.2.1. Binder modification and short-term ageing

The modification protocol and the $CaCO_3$ contents were defined based on studies that also used micro or nanoparticles in asphalt binders (Staub de Melo et al., 2023; Sousa Neto et al., 2022; Zhao et al., 2022; Manfro et al., 2022; Alas et al., 2022; Ramadhansyah et al., 2020; Ashish & Singh, 2019). The procedure followed four steps: (i) the required mass of binder was weighed and transferred to an aluminium beaker; (ii) the binder was gradually heated under progressively increasing mechanical stirring as its viscosity decreased; (iii) the mixing conditions were set at a constant 6,000 rpm and the temperature was raised to 160 °C; and (iv) the modifiers were added continuously and uniformly during the first 30 min of mixing, and the mixing conditions were maintained for a total of 1 h. In the formulations with the reactive terpolymer, the particles and the polymer were added simultaneously, in a distributed manner, during the first 30 min. The selected particle contents were 3%, 7%, and 10% by binder mass, with and without polymer. RET content of 1.8% by binder mass was defined based on Gama (2016) and Queiroz (2022), who identified this percentage as the optimum incorporation content, with phase separation observed at higher polymer dosages. Table 2 presents the nomenclature of the binders produced.

Table 2. Nomenclature and composition of the fourteen binders evaluated in this study.

Nomenclature	Composition
AMP 60/85-E	Commercial polymer-modified binder, high-performance reference
CAP 50/70	Neat binder, base binder of all the formulations
3nC	CAP 50/70 + 3% nano-$CaCO_3$
7nC	CAP 50/70 + 7% nano-$CaCO_3$
10nC	CAP 50/70 + 10% nano-$CaCO_3$
3mC	CAP 50/70 + 3% micro-$CaCO_3$
7mC	CAP 50/70 + 7% micro-$CaCO_3$
10mC	CAP 50/70 + 10% micro-$CaCO_3$
3nC + RET	CAP 50/70 + 3% nano-$CaCO_3$ + 1.8% RET
7nC + RET	CAP 50/70 + 7% nano-$CaCO_3$ + 1.8% RET
10nC + RET	CAP 50/70 + 10% nano-$CaCO_3$ + 1.8% RET
3mC + RET	CAP 50/70 + 3% micro-$CaCO_3$ + 1.8% RET
7mC + RET	CAP 50/70 + 7% micro-$CaCO_3$ + 1.8% RET
10mC + RET	CAP 50/70 + 10% micro-$CaCO_3$ + 1.8% RET

The binders were then subjected to short-term ageing by heat and air in the RTFO to simulate ageing during plant production of asphalt concrete, following ASTM D2872.

2.2.2. Chemical, empirical, and rheological characterisation

The chemical composition of the binders was analysed using Fourier transform infrared spectroscopy (FTIR) to assess potential changes following the incorporation of the particles into the asphalt matrix. The tests were performed in a Bruker FT-IR VERTEX 70 spectrometer, in the region from 500 to 4,000 cm^{-1}, with a resolution of 4 cm^{-1} and 16 scans per spectrum, at the Laboratory of Multifunctional Materials and Numerical Experimentation (LAMMEN-ECT) of the Federal University of Rio Grande do Norte (UFRN), Brazil. The transmittance of each spectrum was normalised between 0 and 1, and the band labels follow the convention ν for a stretching vibration and δ for an angular deformation.

The empirical characterisation comprised penetration (ASTM D5M), softening point (ASTM D36M-14), elastic recovery (DNIT 130/2010-ME; ABNT NBR 15086), and storage stability (163 °C for 72 h in an oven, ASTM D7173). The rheological characterisation comprised rotational viscosity (NBR 15184) and performance grade (PG) determination (ASTM D6373), with calculation of the viscosity ageing index (VAI, Eq. (1)) and of the ageing index (AI, Eq. (2)) (Zhang et al., 2015), before and after RTFO ageing (ASTM D2872), as well as the multiple stress creep and recovery test (MSCR, ASTM D7405). The rheological tests followed the Superpave methodology, using a Discovery HR-1 hybrid rheometer at the Pavement Engineering Laboratory (LEP) of the Federal University of Campina Grande (UFCG), Brazil.

$$VAI\ (\%) = \frac{\eta_{aged} - \eta_{unaged}}{\eta_{unaged}} \times 100 \quad (1)$$

$$AI = \frac{(|G^*|/sin\delta)_{aged}}{(|G^*|/sin\delta)_{unaged}} \quad (2)$$

where η is the rotational viscosity at a given temperature and |G*|/sinδ is the Superpave rutting parameter measured at the PG temperature, in the aged and unaged conditions.

Frequency sweeps within the linear viscoelastic range, established beforehand by a strain sweep, were also run on six binders (CAP 50/70, AMP 60/85-E, 7nC, 7mC, 10nC + RET, and 10mC + RET), before and after RTFO ageing, with 25 mm plates and a 1 mm gap, at frequencies from 0.1 to 100 Hz and temperatures from 5 °C to 65 °C (AASHTO T 315). Master curves of the complex shear modulus |G*| and of the phase angle δ were built by time-temperature superposition at a reference temperature of 25 °C. They are used in Section 3.3.3 to test whether the particles alter the frequency dependence of the modulus at low frequencies, which is the linear viscoelastic signature of a particle network (Lesueur, 2009).

The linear amplitude sweep (LAS) test was performed on RTFO-aged samples following DNIT 439/2022-ME, using 8 mm parallel plates with a 2 mm gap. The procedure consisted of a frequency sweep (0.2 to 30 Hz at 0.1% strain) to obtain the linear viscoelastic parameters, followed by an amplitude sweep (0.1% to 30% strain) at 10 Hz up to fatigue failure. Each LAS test was conducted in duplicate, and the reported values correspond to the average of the two replicates. The results were analysed using the simplified viscoelastic continuum damage (S-VECD) framework, which represents the loss of material integrity (C) as a function of accumulated damage (S) and provides the A and B parameters of the Wöhler curve.

Two failure criteria were adopted. The first is the peak of the stored pseudo-strain energy (PSE), the criterion prescribed by DNIT 439/2022-ME. The stored PSE is the recoverable portion of the energy imposed by the load, computed in the pseudo-strain domain so that the linear viscoelastic response is removed and only the damage remains: it grows while the binder is still able to store energy and decreases once damage prevails, so that its maximum marks the transition from diffuse damage accumulation to macrocrack propagation and defines the fatigue life, N_f. The second is the crack-growth criterion of Hintz and Bahia (2013), in which the crack length inside the specimen is estimated during the amplitude sweep and failure is taken at the critical crack length that marks the onset of rapid crack growth. The two criteria capture different physical events, the loss of the capacity to store energy and the onset of unstable crack propagation, and are therefore reported separately, and the two rankings are compared later, to show whether the standing of a binder depends on how failure is defined. From the Wöhler curves (N_f versus shear strain) obtained with the PSE criterion, the fatigue factor of the binder (FFB) was determined according to Eq. (3) (Martins, 2014; Osmari et al., 2023):

$$FFB = \frac{log\left(N_{f,1.25\%}\right) + log\left(N_{f,2.5\%}\right)}{2} \times \left(log(0.025) - log(0.0125)\right) \quad (3)$$

where $N_{f,1.25\%}$ and $N_{f,2.5\%}$ denote the fatigue life under shear strains of 1.25% and 2.5%, respectively. Higher FFB values indicate greater fatigue resistance. The binders were ranked according to the five performance classes of the Cenpes/Petrobras performance specification proposal, in which the FFB corresponds to the fatigue factor of the binder defined in DNIT 439/2022-ME (Nascimento, 2019, 2020), presented in Table 3. The fatigue results obtained using the PSE criterion were also compared with those derived from the crack-growth failure criterion (Hintz & Bahia, 2013).

Table 3. FFB performance classes at 19 °C (PSE criterion), from the Cenpes/Petrobras performance specification proposal (Nascimento, 2019, 2020).

Class	FFB (PSE, 19 °C)
1 - Low performance	FFB < 1.22
2 - Regular	1.22 ≤ FFB < 1.31
3 - Good	1.31 ≤ FFB < 1.48
4 - Superior	1.48 ≤ FFB < 1.57
5 - High performance	FFB ≥ 1.57

In addition to FFB, alternative LAS indices based on dissipated energy and strain were evaluated. Strain tolerance to failure (ε_T) corresponds to the shear strain at which shear stress decreases to 25% of its peak value in the post-peak portion of the stress-strain curve. Strain energy tolerance (E_f) is the area under the same curve up to this limit. Both indices were proposed by Zhang et al. (2022) to describe the binder's remaining load-carrying capacity after peak stress; higher values indicate greater resistance to fatigue cracking. The Fatigue Resistance Energy Index (FREI, Eq. (4)) is calculated from the pre-peak portion of the curve and combines the shear fracture energy up to peak shear stress, the apparent shear modulus, and the shear strain at 50% of peak shear stress (Zhou et al., 2017). Higher FREI values indicate greater fracture energy and flexibility for a given stiffness, and therefore better cracking resistance. The stress level at peak stored PSE (S_L, Eq. (5)) is the ratio between the shear stress at peak stored PSE and the peak shear stress (Gulzar et al., 2024). Lower S_L values indicate that the binder stores less pseudo-strain energy and

dissipates more energy, which is associated with faster damage accumulation. Two additional indices were used to describe material integrity and degradation. The average reduction in integrity up to failure (I^R, Eq. (6)) expresses the mean loss of pseudo-stiffness accumulated before failure; thus, higher I^R values indicate that the binder can tolerate greater integrity loss before failing (Zhang et al., 2022). The reduction in shear modulus up to peak shear stress ($\Delta|G^*|_{peak(\tau)}$, Eq. (7)) tracks the apparent modulus during the amplitude sweep and quantifies the damage level tolerated before shear resistance begins to decrease (García Mainieri et al., 2021). Higher ε_T, E_f, FREI, I^R, and $\Delta|G^*|_{peak(\tau)}$ values indicate better fatigue resistance, and all are expected to decrease after ageing.

$$FREI = \frac{J_{f-\tau max}}{|G*|_{0.5\tau max}} (\gamma_{0.5\tau max})^2 \quad (4)$$

$$S_L = \frac{\tau_{peak\ stored\ PSE}}{\tau_{peak\ stress}} \times 100 \quad (5)$$

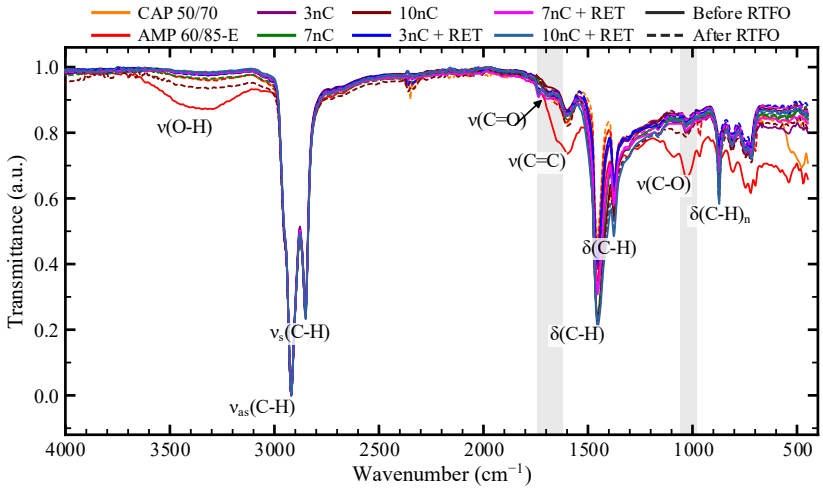
$$I^R = \frac{\int_0^{Nf} (1 - C)\, dN}{Nf} \quad (6)$$

$$\Delta|G^*|_{peak(\tau)} = \frac{|G^*|_{start} - |G^*|_{peak(\tau)}}{|G^*|_{start}} \times 100 \quad (7)$$

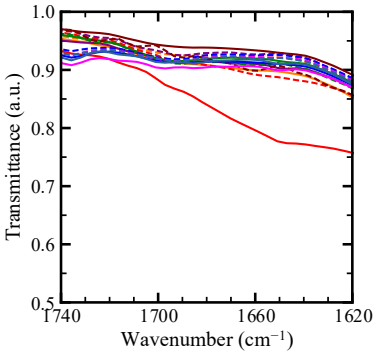
3. Results and discussion

3.1. Chemical characterisation of the modified binders

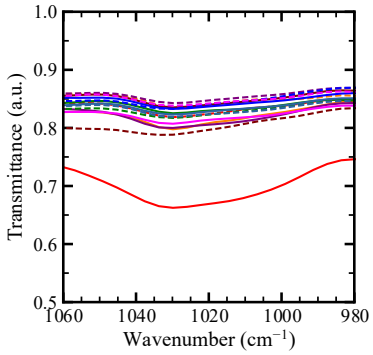
The FTIR spectra of the binders modified with nano-$CaCO_3$ and micro-$CaCO_3$, with and without the terpolymer, are shown in Fig. 7 and Fig. 8, respectively. The main signals indicative of binder composition appear in regions common to hydrocarbon compounds, characterised by high-intensity axial stretching peaks of saturated aliphatic groups between 3,000 and 2,800 cm^{-1}. In this range, peaks at 2,952 cm^{-1} and 2,852 cm^{-1} correspond to asymmetric and symmetric stretching of methyl groups (-CH_3), and peaks at 2,919 cm^{-1} and 2,850 cm^{-1} to asymmetric and symmetric stretching of methylene groups (-CH_2-).



(a)



(b)



(c)

Fig. 7. FTIR spectra of the binders with and without polymer plus nano-$CaCO_3$: (a) full spectra, (b) carbonyl region (1,740 to 1,620 cm^{-1}), and (c) sulfoxide region (1,060 to 980 cm^{-1}).

The spectra show a peak at 1,700 cm^{-1} associated with carbonyl groups (C=O), indicative of oxidation. Peaks characteristic of methylene (1,454 cm^{-1}) and methyl (1,373 cm^{-1}) groups were also identified, in agreement with the C-H stretching at 2,919 cm^{-1} and 2,850 cm^{-1}, together with bands between 1,000 and 1,300 cm^{-1} attributed to C-O bonds. The peaks at 895 and 810 cm^{-1} indicate vibrations of polysubstituted aromatic rings, while the peak at 720 cm^{-1} corresponds to the rocking motion of saturated chains longer than four carbons ($(CH_2)_n$). The O-H (3,000 to 3,600 cm^{-1}) and C=C (around 1,600 cm^{-1}) stretching bands are associated with aromatic unsaturation. The oxidation-related bands (O-H, C=O, and C-O) varied in intensity among the samples without a defined pattern, except in the comparison before and after RTFO. The AMP 60/85-E stood out for a more intense peak at 1,600 cm^{-1} (C=C) and a signal at 986 cm^{-1}, attributed to trans vinyl groups possibly linked to the polymer structure.

In the spectra of Fig. 8, the addition of micro-$CaCO_3$ to the terpolymer produced an increase or emergence of bands in the 1,700 to 1,750 cm^{-1} region, attributed to C=O stretching, indicating the formation of esters or anhydrides after the reaction of the polymer with the binder. Changes in the 1,000 to 1,300 cm^{-1} region, associated with C-O-C (ethers) or C-O (alcohols and esters) bonds, were also verified, suggesting polymerisation reactions or chemical modification of the matrix. In addition, the reduction or disappearance of bands attributed to functional groups of the neat polymer indicates the consumption of those groups in chemical reactions with the binder. These spectroscopic observations indicate that the reactive terpolymer acted not only as a physical modifier but also as a chemical modifier, improving the compatibility and stability of the modified binder. The presence of the carbonate group (CO_3^{2-}) was confirmed by its characteristic asymmetric stretching bands between 1,400 and 1,500 cm^{-1} and by an intense angular deformation band around 870 cm^{-1}, both of which were intensified after the addition of the mineral, indicating its incorporation into the binder.

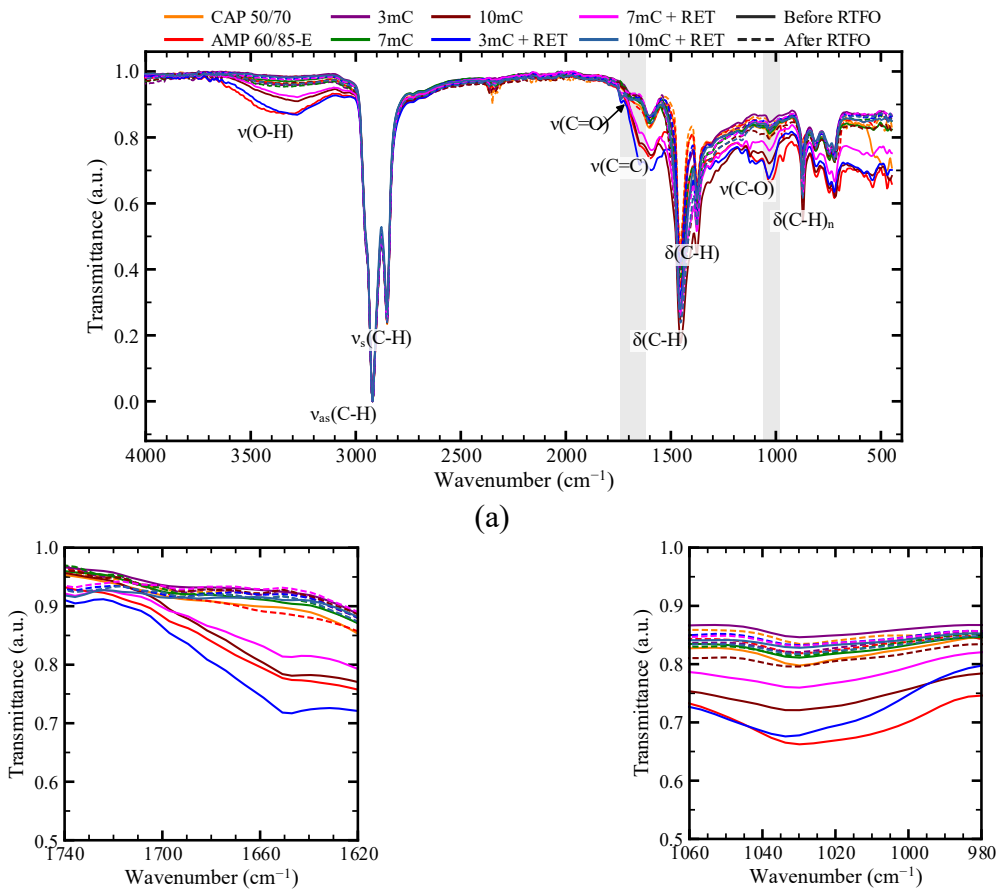


Fig. 8. FTIR spectra of the binders with and without polymer plus micro-$CaCO_3$: (a) full spectra, (b) carbonyl region (1,740 to 1,620 cm^{-1}), and (c) sulfoxide region (1,060 to 980 cm^{-1}).

Table 4 presents the oxidation indices computed from the areas of the hydroxyl (3,100 to 3,600 cm^{-1}) and carbonyl (1,700 cm^{-1}) peaks relative to the total area of each spectrum. The reference binders behaved differently: CAP 50/70 showed greater susceptibility to oxidation than AMP 60/85-E, confirming the higher oxidative stability of the polymer-modified binder, as reported by Lu and Isacsson (2002). In the binders with particles and without the terpolymer, the oxidation indices remained similar to those of CAP 50/70 (0.015 to 0.029), indicating that, at the evaluated contents (3%, 7%, and 10%), the isolated addition of the particles did not produce a significant barrier against oxidative reactions. In contrast, the incorporation of RET reduced the oxidation indices to I1700 = 0.012 and I3600 = 0.023 in all six systems, corresponding to decreases of approximately 20% and 21% in the two indices relative to the binders without RET, and matching the values of AMP 60/85-E. For the systems with RET, the carbonyl index is not a direct measure of oxidation, since the ester groups of the terpolymer absorb in the same region as the carbonyl groups formed on ageing. These findings agree with Oliveira (2022), who also observed lower formation of oxidative groups in binders modified with reactive terpolymers after ageing. The spectra are not sensitive to residual reactive groups: at 1.8% of terpolymer with 6% GMA, the epoxide content of the binder is about 0.1% by mass, and the epoxide ring bands near 910 and 845 cm^{-1} overlap with the out-of-plane aromatic C-H bands of the binder at 895 and 810 cm^{-1}, so the consumption of the GMA groups is inferred from the ester and ether bands discussed above.

Table 4. Oxidation indices of the binders.

Sample	I_{1700}	I_{3600}
AMP 60/85-E	0.012	0.023
CAP 50/70	0.015	0.029
3nC	0.015	0.029
7nC	0.015	0.028
10nC	0.015	0.029
3mC	0.015	0.029
7mC	0.015	0.029
10mC	0.015	0.029
3nC + RET	0.012	0.023
7nC + RET	0.012	0.023
10nC + RET	0.012	0.023
3mC + RET	0.012	0.023
7mC + RET	0.012	0.023
10mC + RET	0.012	0.023

3.2. Empirical characterisation of the modified binders

Table 5 presents the results of tests evaluating the physical and empirical properties of the modified binders before and after RTFO ageing.

Table 5. Empirical characterisation of the binders.

Sample	PEN	RET PEN (%)	SP (°C)	SP increase (°C)	TSI	Mass loss (%)	ER (%)
Before RTFO							
AMP 60/85-E	41	-	60	-	0.56	-	86.0
CAP 50/70	59	-	48	-	-1.33	-	-
3nC	57	-	52.5	-	-0.27	-	-
7nC	54	-	54	-	-0.05	-	-
10nC	55	-	53	-	-0.24	-	-
3mC	55	-	52	-	-0.48	-	-
7mC	54	-	52.5	-	-0.41	-	-
10mC	52	-	54	-	-0.15	-	-
3nC + RET	42	-	60.25	-	0.66	-	75.5
7nC + RET	39	-	62	-	0.62	-	75.5
10nC + RET	36	-	62	-	0.64	-	75.5
3mC + RET	44	-	59	-	0.52	-	76.0
7mC + RET	40	-	60.75	-	0.65	-	76.0
10mC + RET	38	-	61.5	-	0.67	-	76.0
After RTFO							
AMP 60/85-E	30	73	67	7.0	-	0.01	-
CAP 50/70	41	69	52	4.0	-	0.33	-
3nC	47	82	57	4.5	-	0.12	-
7nC	45	83	60	6.0	-	0.07	-
10nC	46	84	58.5	5.5	-	0.08	-
3mC	47	85	56.5	4.5	-	0.12	-
7mC	46	85	58.75	6.3	-	0.13	-
10mC	41	79	61	7.0	-	0.10	-
3nC + RET	34	81	65	4.8	-	0.09	-
7nC + RET	32	82	65.5	3.5	-	0.09	-

10nC + RET	31	86	69	7.0	-	0.07	-
3mC + RET	37	84	63.75	4.8	-	0.01	-
7mC + RET	34	85	65.5	4.8	-	0.01	-
10mC + RET	33	87	65	3.5	-	0.09	-

PEN = penetration (0.1 mm); RET PEN = retained penetration; SP = softening point; TSI = thermal susceptibility index; ER = elastic recovery.

The reference binders showed the expected behaviour, with penetration decreasing after RTFO ageing within the range reported in the literature (Rahim et al., 2024; Albayati et al., 2024). Adding micro- or nanoparticles alone moderately reduced penetration, with decreases from 3.4% to 11.9%; among the polymer-free binders, 10mC was the stiffest, and penetration decreased consistently as the micro-$CaCO_3$ content increased. The incorporation of RET produced a stronger hardening effect, reducing penetration to 36–44 (0.1 mm) and making the nano-$CaCO_3$ systems comparable to aged AMP 60/85-E. Compared with AMP 60/85-E, 7mC + RET and 7nC + RET showed reductions of about 2.4% and 4.9%, respectively, while the greatest hardening occurred for 10mC + RET and 10nC + RET, with reductions of about 7.3% and 12.2%.

Retained penetration reflects the binder's ability to preserve its consistency after RTFO ageing; higher values indicate lower ageing sensitivity. ANP Resolution No. 897/2022 establishes a minimum value of 55% for CAP 50/70, and all binders met this requirement. The particles alone raised the retained penetration from 69% for CAP 50/70 to 82% to 84% for the nano-$CaCO_3$ binders and 79% to 85% for the micro-$CaCO_3$ binders, above the 73% of AMP 60/85-E and with no consistent dependence on content. The terpolymer systems reached 81% to 87%, so on this index the terpolymer adds little to what the particles already produce, and the gain in ageing resistance measured by retained penetration is attributable mainly to the particles.

For the softening point, ANP Resolution No. 897/2022 sets minimum values of 48 °C for CAP 50/70 and 60 °C for AMP 60/85-E, met by all binders. The AMP 60/85-E presented a higher softening point than CAP 50/70 before and after ageing. The addition of nano-$CaCO_3$ raised the softening point moderately (approximately 4 to 6 °C), without relevant differences among contents, and all micro-$CaCO_3$ contents also increased the softening point relative to CAP 50/70. The terpolymer produced the largest increases, reaching 69 °C after RTFO for 10nC + RET and 65.0 °C for 10mC + RET. Only 10nC + RET exceeded the aged AMP 60/85-E (67 °C). Within the nano series the softening point rose with the particle content (65.0, 65.5, and 69.0 °C at 3%, 7%, and 10%), whereas the micro series showed no such trend (63.75, 65.5, and 65.0 °C).

The thermal susceptibility index (TSI) shows that CAP 50/70 (-1.33) is the most susceptible binder to thermal variation, while AMP 60/85-E (+0.56) presents better thermal stability. The particles reduced the thermal susceptibility, with the best performance at 7% content for the nanoparticles and at 10% for the microparticles. With the addition of RET, all systems reached TSI values between +0.52 and +0.67, practically eliminating differences among particle types and contents and matching or exceeding AMP 60/85-E (+0.56), the exception being 3mC + RET (+0.52). In the particle-RET systems the TSI is therefore set by the terpolymer, and neither the particle type nor the content changes it.

CAP 50/70 presented the highest mass loss (0.33%), indicating greater susceptibility to ageing, although within the normative limit, whereas AMP 60/85-E lost only 0.01%. The addition of nanoparticles substantially reduced mass loss, with the best result at 7% content, and the incorporation of RET maintained or improved this resistance (0.07% for 10nC + RET). Among the microparticle formulations, 10mC exhibited the lowest mass loss, although the lowest value of all the polymer-free binders was that of 7nC (0.07%). Although the differences among binders are

small in practical terms, the RET systems reached values close to AMP 60/85-E (0.01% for 3mC + RET and 7mC + RET). All binders met ANP Resolution No. 897/2022, and the lower mass losses observed in the modified systems indicate greater resistance to volatilization.

According to ANP Resolution No. 897/2022, the classification of elastomeric binders is based on the softening point and on the elastic recovery, whose minimum value is 85% for the 60/85-E class. The AMP 60/85-E meets this requirement, and the addition of 1.8% RET raised the elastic recovery of the modified binders to approximately 76%, indicating improved elastomeric behaviour relative to conventional binders, although still below AMP 60/85-E. Increasing the $CaCO_3$ content did not alter elastic recovery, indicating that the elasticity conferred by RET is preserved even as stiffness increases.

Table 6 presents the storage stability results, expressed as the difference between the softening points measured at the top and bottom of the storage tube. All binders exhibited a temperature difference below the 5 °C limit specified in ASTM D7173, indicating the absence of phase separation. The binders with particles alone showed adequate stability (1.0 to 3.0 °C), with a slight tendency towards sedimentation and, for the microparticles, differences that increased progressively with content, from 1.5 °C at 3% to 3.0 °C at 10%. The combination with RET reduced the differences further (0.5 to 1.5 °C), with the 3nC + RET system standing out at 0.5 °C and the 7mC + RET system at 1.0 °C, both below the AMP 60/85-E reference (2.0 °C). These results agree with Zhang (2019), who reported that reactive polymers reduce phase separation and increase homogeneity. RET therefore improves the binder's physical stability during prolonged storage, in addition to its mechanical and thermal performance.

Table 6. Storage stability results.

Sample	SP top (°C)	SP bottom (°C)	Difference (°C)
AMP 60/85-E	61.0	63.0	2.0
CAP 50/70	-	-	-
3nC	53.0	54.0	1.0
7nC	54.0	55.0	1.0
10nC	53.0	54.5	1.5
3mC	52.5	54.0	1.5
7mC	53.0	55.0	2.0
10mC	55.0	58.0	3.0
3nC + RET	61.0	61.5	0.5
7nC + RET	63.0	64.0	1.0
10nC + RET	63.5	65.0	1.5
3mC + RET	60.5	62.0	1.5
7mC + RET	62.0	63.0	1.0
10mC + RET	63.5	65.0	1.5

SP = softening point.

3.3. Rheological characterisation of the modified binders

3.3.1. Consistency, ageing, and permanent deformation

Table 7 presents the results of the rheological tests used to determine the properties of the binders modified with nano-$CaCO_3$ and micro-$CaCO_3$, before and after RTFO ageing.

Table 7. Rheological characterisation of the binders: reference binders and binders modified with $CaCO_3$ particles only.

Test	AMP 60/85-E	CAP 50/70	3nC	7nC	10nC	3mC	7mC	10mC

Before RTFO								
RV 135 °C (cP)	1060	377	514	627	614	540	611	604
RV 150 °C (cP)	496	188	249	298	297	259	294	287
RV 177 °C (cP)	178	69	88	102	105	92	102	101
PG	70	64	70	70	70	64	70	70
Continuous PG (°C)	75.4	66.7	70.7	72.7	70.6	69.9	72.0	70.9
After RTFO								
RV 135 °C (cP)	2000	500	645	770	754	669	737	734
RV 150 °C (cP)	870	241	301	357	356	315	346	344
RV 177 °C (cP)	278	85	104	118	121	107	118	118
PG	70	64	70	70	70	64	70	70
Continuous PG (°C)	72.8	62.6	69.8	71.9	69.5	67.5	71.2	69.2
$Jnr_{0.1}$ (1/kPa)	0.8	4.2	3.2	2.6	3.0	2.6	2.5	2.4
$Jnr_{3.2}$ (1/kPa)	1.1	4.4	3.5	2.8	3.3	2.8	2.7	2.6
Traffic designation	H	S	S	S	S	S	S	S
Jnr,diff (%)	48.7	5.0	7.7	7.3	8.9	7.0	9.4	7.5
VAI 135 °C (%)	89	33	25	23	23	24	21	22
VAI 150 °C (%)	75	28	21	20	20	21	18	20
VAI 177 °C (%)	55	23	18	15	15	17	15	17
AI	1.66	2.07	1.74	1.72	1.73	1.95	1.94	1.91

Table 7 (continued). Rheological characterisation of the binders: binders modified with $CaCO_3$ particles and 1.8% RET.

Test	3nC + RET	7nC + RET	10nC + RET	3mC + RET	7mC + RET	10mC + RET
Before RTFO						
RV 135 °C (cP)	1186	1450	1300	1041	1141	1272
RV 150 °C (cP)	575	698	625	517	562	627
RV 177 °C (cP)	202	250	219	191	207	237
PG	70	70	70	70	70	70
Continuous PG (°C)	74.0	75.7	75.9	75.0	72.8	75.5
After RTFO						
RV 135 °C (cP)	1784	2262	1753	1650	1495	1989
RV 150 °C (cP)	813	1025	811	749	697	923
RV 177 °C (cP)	265	335	268	247	233	311
PG	70	70	70	70	70	70
Continuous PG (°C)	72.9	75.0	74.9	73.2	71.5	73.7
$Jnr_{0.1}$ (1/kPa)	1.0	0.9	0.7	1.0	1.0	0.8
$Jnr_{3.2}$ (1/kPa)	1.2	1.1	0.9	1.2	1.2	0.9
Traffic designation	H	H	V	H	H	V
Jnr,diff (%)	25.9	17.0	13.0	12.0	13.3	3.2
VAI 135 °C (%)	50	56	35	59	31	56
VAI 150 °C (%)	41	47	30	45	24	47
VAI 177 °C (%)	31	34	22	29	13	32
AI	1.56	1.55	1.59	1.54	1.50	1.53

RV = rotational viscosity; PG = performance grade; Jnr = non-recoverable creep compliance at 0.1 and 3.2 kPa; Jnr,diff = stress sensitivity; VAI = viscosity ageing index; AI = ageing index.

CAP 50/70, the least viscous binder evaluated, showed an increase in viscosity with the addition of nano- and microparticles at all temperatures, and the RTFO raised the viscosity of all binders, as expected from ageing-induced stiffening. The binders with 3%, 7%, and 10% nano-$CaCO_3$ combined with 1.8% RET exhibited viscosities higher than those of AMP 60/85-E before ageing, and 7nC + RET was the only binder of the study to remain above AMP 60/85-E after the RTFO as well (2262 cP against 2000 cP at 135 °C). Among the microparticle systems, 7mC + RET and 10mC + RET also exceeded AMP 60/85-E before ageing, but none of them did so after

the RTFO. Higher viscosities indicate greater resistance to flow under shear, which may favour rutting performance, as reported for other particle-modified binders (Zhang et al., 2021; Albayati et al., 2024). Conversely, higher viscosity may require higher mixing and compaction temperatures, reducing workability and increasing energy consumption.

The viscosity ageing index (VAI) decreased progressively with temperature for all samples. AMP 60/85-E showed the highest percentages, from 89% at 135 °C to 55% at 177 °C, while CAP 50/70 remained between 33% and 23%. The particle systems without RET exhibited the lowest values, between 15% and 25%, whereas incorporating RET raised the VAI to between 13% and 59% depending on the formulation and the temperature. Even so, RET systems remained below the AMP 60/85-E reference at every content and temperature.

The VAI and the AI point in opposite directions for the RET systems, and the divergence deserves a word. Those binders show the largest relative viscosity increase on ageing among the modified binders, from 13% to 59%, yet the lowest ageing indices (1.50 to 1.59, against 1.72 to 1.95 for the particle-only systems) and the lowest oxidation indices (Table 4). The two indices are measured in different regimes. The VAI compares rotational viscosities between 135 °C and 177 °C, where the binder is a fully viscous liquid and any glycidyl methacrylate groups left after mixing are able to react with the matrix (Duarte et al., 2023), so part of the increase recorded after the RTFO may reflect further reaction rather than oxidation. The AI compares the rutting parameter at the PG temperature, inside the linear viscoelastic range and close to the temperature at which the binder works. The reading is supported by the agreement among the three indicators measured at or near service temperature (the AI, the mass loss, and the retained penetration), which disagree with the VAI. The AI is therefore taken as the ageing indicator for these binders, and the VAI is excluded from the composite ranking presented later; including it would not alter the standing of the RET systems relative to AMP 60/85-E, which has the highest VAI of the fourteen binders.

The PG results show that the modified binders without polymer performed better than CAP 50/70, whose continuous grade dropped after the RTFO. One hypothesis for this improvement is that the $CaCO_3$ particles reduce the volatilization of light fractions and contribute to the rheological stability of the binder, which is consistent with the lower mass loss of these binders after the RTFO (Table 5). With the addition of RET, five of the six systems reached continuous grades at or above the 72.8 °C of the aged AMP 60/85-E, the exception being 7mC + RET (71.5 °C); before the RTFO, three of the six remained below the 75.4 °C of AMP 60/85-E. The gain is consistent with the reactive character of the terpolymer (Duarte et al., 2023; Oliveira, 2022).

The ageing index (AI) confirms this picture. CAP 50/70 presented the highest value (2.07), indicating high susceptibility to thermal ageing, in agreement with Airey (2003), who highlights the greater oxidation sensitivity of conventional binders. AMP 60/85-E reached 1.66, consistent with the reduced mobility of volatile fractions in polymer-modified binders (Yao et al., 2013; Lu & Isacsson, 2002). The nano-$CaCO_3$ systems presented values between 1.72 and 1.74, a slight improvement consistent with a physical barrier effect against oxidation, while the micro-$CaCO_3$ systems showed higher indices (1.91 to 1.95), indicating lower efficiency. RET formulations reached the lowest values (1.50 to 1.59), with 7mC + RET standing out (1.50), an effect attributed to the reactive action of the terpolymer, which increases structural cohesion and reduces oxidation, in line with Oliveira (2022). The proximity among the RET values (1.50 to 1.59) indicates that, within these systems, the particle type and content do not change the ageing index.

The resistance to permanent deformation was evaluated through the non-recoverable creep compliance Jnr at 0.1 and 3.2 kPa, following the Superpave framework. The addition of particles to CAP 50/70 reduced Jnr, indicating improved rutting resistance, with emphasis on 7nC ($Jnr_{3.2}$ =

2.8 1/kPa) and 10mC ($Jnr_{3.2}$ = 2.6 1/kPa). However, these values remain above those obtained for AMP 60/85-E ($J_{nr3.2}$ = 1.1 1/kPa). The reduction of J_{nr} with increasing particle content is near-linear for the microparticles (2.8, 2.7, and 2.6 1/kPa at 3%, 7%, and 10%) but not for the nanoparticles (3.5, 2.8, and 3.3 1/kPa). The incorporation of RET led to much larger gains. The best results were obtained at the highest content, with 10mC + RET and 10nC + RET reaching $J_{nr3.2}$ = 0.9 1/kPa, below the 1.1 1/kPa of AMP 60/85-E, while 3nC + RET, 3mC + RET, and 7mC + RET remained marginally above it at 1.2 1/kPa. Adding the terpolymer to a particle-modified binder therefore lowers $J_{nr3.2}$ by a factor of 2.3 to 3.7, from 2.6 to 3.5 1/kPa to 0.9 to 1.2 1/kPa, whereas raising the particle content from 3% to 10% within the RET systems lowers it by 0.3 1/kPa, in both the micro and the nano series; the terpolymer accounts for most of the gain, in agreement with Zhang et al. (2021) and Yao et al. (2013), and the particles remain active in its presence. Regarding the traffic designation (AASHTO M 332), the systems without polymer kept the S class of CAP 50/70, while the RET formulations reached the H class and, for 10nC + RET and 10mC + RET, the very heavy class (V), exceeding AMP 60/85-E. AASHTO M 332 also limits the stress sensitivity $J_{nr,diff}$ to 75%, to screen binders whose compliance grows disproportionately between 0.1 and 3.2 kPa; a low $J_{nr,diff}$ means that the binder keeps the rutting resistance measured at 3.2 kPa when the stress imposed by slow, heavy, or channelised traffic exceeds that level. All binders met the limit; the systems without polymer became somewhat more stress sensitive than CAP 50/70, whereas the RET systems showed decreasing sensitivity as the particle content increased, a behaviour also reported in the literature (Melo Neto et al., 2020; Wang et al., 2021; Zhang et al., 2018; Marinho Filho et al., 2020; Sousa Neto et al., 2023). The stress sensitivity also separates the two references sharply. AMP 60/85-E has a $J_{nr,diff}$ of 48.7%, within the limit but two to fifteen times that of the RET systems (3.2% to 25.9%). Its non-recoverable compliance therefore grows with applied stress much faster than that of the RET systems, so the advantage it holds at 3.2 kPa would narrow at higher stress levels. For heavily loaded pavements, where the stress carried by the binder may exceed the 3.2 kPa of the test, this is a point in favour of the RET formulations.

3.3.2. Fatigue behaviour from LAS test results

The fatigue behaviour is examined under the two failure criteria, the peak of the stored pseudo-strain energy and the crack-growth criterion of Hintz and Bahia (2013), and complemented by the alternative LAS indices I^R, ε_T, E_f, FREI, S_L, and $\Delta|G^*|_{peak(\tau)}$.

The integrity (C) versus accumulated damage (S) curves obtained with the PSE model are shown in Fig. 9. The curves fall within a narrow band and are ordered differently from the fatigue lives. AMP 60/85-E and 7mC lose integrity most slowly (C = 0.5 is reached at S = 50 and 48), CAP 50/70, 7nC, and 10nC most quickly (S = 34 to 35), and the six RET systems lie in between (S = 36 to 42), overlapping 3nC, 3mC, and 10mC (36 to 43). The C versus S curve describes how much integrity is lost per unit of damage, not how fast damage accumulates under a given strain: the polymer network of AMP 60/85-E shows here as a slower loss of integrity, consistent with a more elastic and more resilient matrix, but the longer fatigue lives of the RET systems relative to the particle-only systems (Table 8) do not come from a slower loss of integrity per unit of damage, since their curves overlap. They come from the other terms of the S-VECD prediction, the linear viscoelastic properties and the damage evolution rate obtained in the frequency sweep, and from the position of the PSE peak. The curves therefore do not by themselves separate the polymer systems from the particle-only systems, and the comparison between formulations rests on the fatigue lives and on the indices of Tables 8 and 9. The slower integrity loss of 3nC and 3mC

relative to CAP 50/70 is consistent with studies reporting reduced integrity loss with accumulated damage and fatigue-life gains with the addition of nanosilica (He et al., 2021).

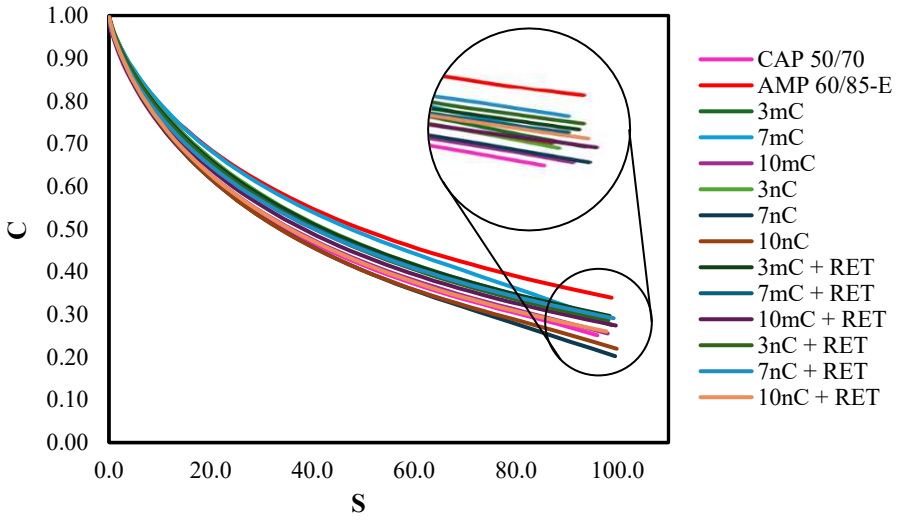


Fig. 9. Integrity (C) versus accumulated damage (S) curves based on the PSE criterion.

Table 8 summarises the FFB and the fatigue life at 19 °C under both criteria. Higher FFB values are desirable, since they indicate greater resistance to fatigue cracking (Martins, 2014; Bessa et al., 2019; Possebon, 2021; Osmari et al., 2023; Rocha et al., 2024; Enríquez-León et al., 2025). AMP 60/85-E is the best binder under both criteria (FFB = 1.54 and $N_{f,1.25\%}$ = 3.68E+05 with PSE; FFB = 1.36 and $N_{f,1.25\%}$ = 9.06E+04 with crack growth), and CAP 50/70 the worst. The two criteria agree on the references and disagree on the modified binders. Under the PSE criterion the best modified binder is 3nC + RET ($N_{f,1.25\%}$ = 3.04E+05, 4.5 times CAP 50/70 and 83% of AMP 60/85-E), and the fatigue life falls as the nanoparticle content rises, with and without RET. Under the crack-growth criterion the best is 7nC + RET ($N_{f,1.25\%}$ = 6.46E+04, 2.0 times CAP 50/70), and 3nC + RET drops to the middle of the series. The particle-only systems gain 59% to 105% over CAP 50/70 under the PSE criterion, and the micro systems reach their maximum at 7%, not at 10%. A plausible cause of the loss of efficiency at higher nanoparticle contents is agglomeration (Xu et al., 2018), which the TEM images show in the dry product (Fig. 5); the hypothesis is examined against the linear viscoelastic master curves together with the alternative LAS indices. The disagreement between the criteria is quantified in the next section.

Table 8. FFB and fatigue life at 19 °C under the two failure criteria.

Sample	FFB (PSE)	Nf (1.25%)	Nf (2.50%)	Class (PSE)	FFB (crack)	Nf (1.25%)	Nf (2.50%)
AMP 60/85-E	1.54	3.68E+05	4.97E+04	4 - Superior	1.36	9.06E+04	1.22E+04
CAP 50/70	1.34	6.79E+04	1.14E+04	3 - Good	1.24	3.28E+04	5.50E+03
3nC	1.42	1.39E+05	1.91E+04	3 - Good	1.27	4.57E+04	6.30E+03
7nC	1.38	1.08E+05	1.30E+04	3 - Good	1.20	2.74E+04	3.30E+03
10nC	1.39	1.12E+05	1.50E+04	3 - Good	1.19	2.43E+04	3.24E+03
3mC	1.39	1.14E+05	1.60E+04	3 - Good	1.27	4.31E+04	6.05E+03
7mC	1.40	1.20E+05	1.62E+04	3 - Good	1.24	3.58E+04	4.81E+03
10mC	1.40	1.15E+05	1.66E+04	3 - Good	1.25	3.88E+04	5.61E+03
3nC + RET	1.52	3.04E+05	3.96E+04	4 - Superior	1.27	4.71E+04	6.13E+03
7nC + RET	1.49	2.45E+05	3.30E+04	4 - Superior	1.32	6.46E+04	8.72E+03

10nC + RET	1.49	2.46E+05	3.18E+04	4 - Superior	1.25	3.81E+04	4.93E+03
3mC + RET	1.47	2.10E+05	2.78E+04	3 - Good	1.27	4.58E+04	6.05E+03
7mC + RET	1.47	2.02E+05	2.92E+04	3 - Good	1.26	4.01E+04	5.79E+03
10mC + RET	1.47	1.98E+05	2.74E+04	3 - Good	1.26	3.99E+04	5.51E+03

FFB = fatigue factor of the binder; N_f = fatigue life. The classification follows the FFB classes of Table 3, which were calibrated for the PSE criterion only and are therefore not applied to the crack-growth results.

Fig. 10 presents the stress-strain response of the binders in the LAS test. The peak shear stress measures the stiffness the binder reaches before damage prevails, and it is not by itself a fatigue indicator: AMP 60/85-E, the binder with the longest fatigue life under both criteria, has the lowest peak stress of the whole set (0.74 MPa), below the 0.79 MPa of the neat CAP 50/70. The particles raise the peak stress, which is the expected reinforcing effect of a rigid filler: 10nC reaches 1.18 MPa, about 50% above CAP 50/70, and the micro-$CaCO_3$ systems exceed 1.0 MPa from 7% content. The nano systems at 7% and 10% reach the peak earlier, at 6.9% and 7.1% strain, against 8.0% for 7mC and 10mC and 8.8% for CAP 50/70, so the stress decay starts at a smaller strain even though the peak stress itself is similar (1.01 MPa for both 7nC and 7mC). Adding RET does not raise the peak stress further, and in the nano series it lowers it (10nC + RET reaches 1.12 MPa against 1.18 MPa for 10nC). What RET changes is the post-peak branch. The strain tolerance ε_T, which is the strain at which the stress has fallen to a quarter of its peak, rises from 14.5% to 16.1% for the particle-only systems to 21.7% to 23.6% for the systems with RET (Table 9), against 25.6% for AMP 60/85-E, so the binder keeps carrying load over a much wider strain range. Yu et al. (2023) highlight the role of reactive polymers in forming stronger and more compatible networks.

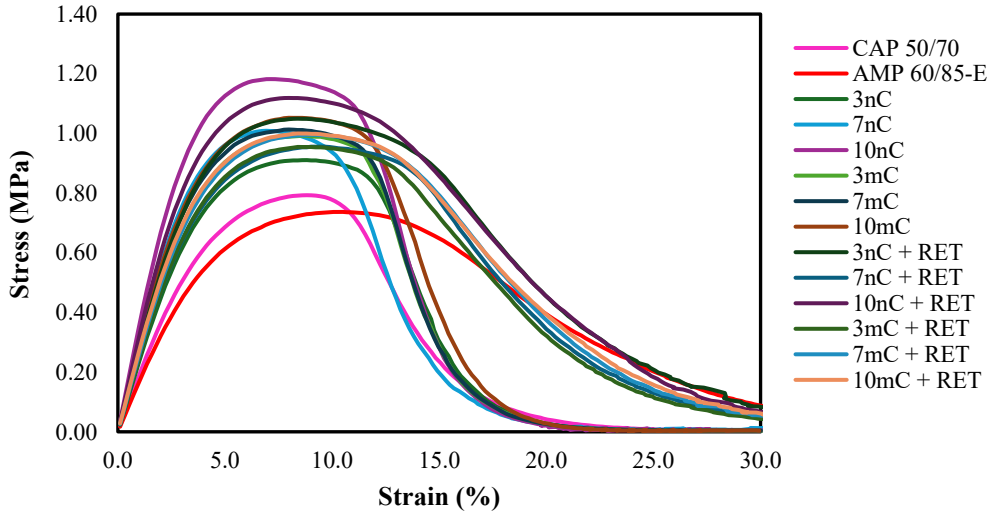
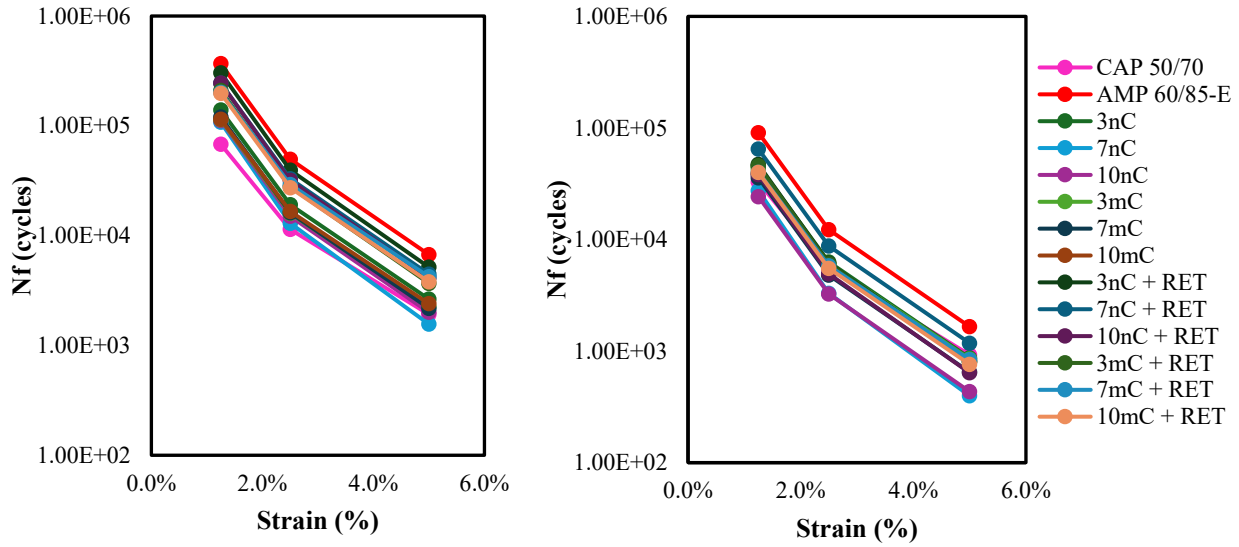


Fig. 10. Stress-strain response in the LAS test for the binders without and with polymer.

Fig. 11 presents the Wöhler curves under the two criteria. AMP 60/85-E leads across the whole strain range in both panels, and the gap widens with the strain amplitude, the expected signature of an elastomeric network that delays crack propagation. RET systems form a distinct band above the particle-only systems under the PSE criterion, whereas under the crack-growth criterion the band narrows and overlaps the best particle-only systems, 3nC and 3mC; the particle-only systems remain close to CAP 50/70 in both panels. What changes between the panels is the order inside the RET band: 3nC + RET leads under the PSE criterion and falls behind 7nC + RET

under the crack-growth criterion, whose fatigue life is 136% above that of 7nC. The nanoparticles surpass the microparticles at 3% content, by 22% in fatigue life, but not at 7% and 10%, where the microparticle systems are ahead.



(a) (b)

Fig. 11. Wöhler curves of the binders: (a) PSE criterion, (b) crack-growth criterion**.**

Table 9 presents the alternative LAS indices. AMP 60/85-E shows the best overall balance, with high E_f (1.31E+07 Pa), high ε_T (25.64%), FREI of 1.80, $\Delta|G^*|_{peak(\tau)}$ of 59.11%, and I^R of 0.296, indicating equilibrium among stiffness, deformability, fatigue resistance, and healing potential. In the nano-$CaCO_3$ systems, low contents (3%) raise E_f moderately without penalizing the FREI. At 7% the E_f does not change (1.07E+07 Pa, the same value as at 3%) and at 10% it rises to 1.34E+07 Pa, but in both cases the FREI collapses to about 0.45. The collapse is not the signature of a percolating particle network. The |G*| and δ master curves after the RTFO (CAP 50/70, AMP 60/85-E, 7nC, 7mC, 10nC + RET, and 10mC + RET) show why: such a network raises the storage modulus and flattens its frequency dependence at low frequencies (Lesueur, 2009), whereas the curves of 7nC and 7mC differ by less than 12% in |G*| (ratio 0.98 to 1.12) and by at most 1.1° in δ over the whole reduced-frequency range, both raise |G*| by a factor of 1.2 to 2.6 relative to CAP 50/70 with a reduction of up to 7° in δ, and at the lowest reduced frequencies both return to the near-viscous phase angles of CAP 50/70 (82° to 90°), while AMP 60/85-E and the RET systems remain well below that level over most of the same range (66° to 78°). The linear viscoelastic response therefore shows no stiffening network at 7% for either product and does not distinguish the nano- from the micro-$CaCO_3$ binder; whatever distinguishes them acts only once damage starts. The FREI falls because the stress peak is reached at a smaller strain (6.9% for 7nC against 8.0% for 7mC, Fig. 10) at a similar peak stress, which reduces the fracture energy accumulated up to the peak while the modulus and the strain at half the peak stress are unchanged. The nano-specific effect is therefore confined to the damage regime, which is consistent with stress concentration at agglomerates of the kind shown in Fig. 5. The addition of RET improves the nano-$CaCO_3$ systems substantially, especially 7nC + RET (FREI = 1.18; E_f = 1.50E+07 Pa; ε_T = 21.95%; $\Delta|G^*|_{peak(\tau)}$ = 60.28%), indicating higher fatigue resistance and healing potential.

The binders modified only with micro-$CaCO_3$ depend on the modifier concentration, with trends opposite to those observed at the nanoscale. The FREI decreases as the content increases, from 0.81 for 3mC to 0.71 for 10mC, showing that a higher particle load does not improve fatigue resistance despite the near-linear growth of E_f (from 1.13E+07 Pa to 1.26E+07 Pa). This suggests that the microparticles act predominantly as an inert filler, without establishing effective reinforcing networks, and the stability of $\Delta|G^*|_{peak(\tau)}$ (around 57%) corroborates the limited interaction with the asphalt matrix. The addition of RET raised the mean strain tolerance of the microparticle systems by about 43%, from ε_T = 15.64% for 3mC, 7mC, and 10mC to 22.31% for the corresponding systems with RET, and raised the mean FREI by about 29%, from 0.75 to 0.96. The largest individual gain was observed for the pair 7mC and 7mC + RET, whose FREI increased from 0.71 to 1.10, a 55% increase. A possible reading is that RET acts as an interfacial plasticizing agent, compensating for the stiffness induced by the microparticles, which is consistent with the strain tolerance of the RET systems being nearly independent of the particle content (Table 10).

The IR is the average reduction in integrity accumulated up to failure, so that higher values indicate a binder that can tolerate a greater loss of integrity before failing (Zhang et al., 2022). CAP 50/70 presented I^R = 0.263, below the 0.296 of AMP 60/85-E. The highest single value was reached by 7nC + RET (0.313), but 10mC, which carries no polymer, reaches 0.309 and stands above five of the six systems with RET, so the index does not separate the polymer systems from the others. The S_L is lower for the systems with RET (85% to 91%) than for those with particles alone (90% to 94%), which means that they reach the peak of the stored energy at a smaller fraction of their peak stress and therefore dissipate a larger share of the imposed energy; it is the one index on which RET systems do not lead. Overall, an optimum balance appears at intermediate contents, and 7nC + RET stands out as the most balanced formulation (high FREI, ε_T, I^R, and $\Delta|G^*|_{peak(\tau)}$), especially for applications with high fatigue demand.

Table 9. Alternative LAS indices of the binders.

Sample	I^R	ε_T (%)	E_f (Pa)	FREI	$\Delta\|G^*\|_{peak(\tau)}$ (%)	S_L (%)
AMP 60/85-E	0.296	25.64	1.31E+07	1.80	59.11	86.85
CAP 50/70	0.263	15.69	8.65E+06	1.12	53.98	92.87
3nC	0.270	15.82	1.07E+07	1.04	55.94	92.13
7nC	0.250	14.53	1.07E+07	0.44	52.74	91.84
10nC	0.261	15.04	1.34E+07	0.45	54.54	90.46
3mC	0.273	15.44	1.13E+07	0.81	56.64	93.94
7mC	0.290	15.40	1.17E+07	0.71	57.36	93.38
10mC	0.309	16.09	1.26E+07	0.71	56.57	91.80
3nC + RET	0.272	23.57	1.75E+07	0.78	56.13	85.72
7nC + RET	0.313	21.95	1.50E+07	1.18	60.28	90.12
10nC + RET	0.283	23.24	1.82E+07	0.71	57.11	85.10
3mC + RET	0.266	21.74	1.47E+07	1.01	54.79	91.47
7mC + RET	0.279	22.38	1.58E+07	1.10	58.64	87.43
10mC + RET	0.287	22.80	1.61E+07	0.77	57.18	89.49

IR = integrity reduction index; ε_T = strain tolerance; E_f = strain energy tolerance; FREI = Fatigue Resistance Energy Index; SL = stored PSE stress level.

3.4. Criterion dependence and comparative ranking of the formulations

The failure criteria do not rank the formulations in the same order, and neither do the distress families. Over the twelve modified binders, the Spearman rank correlation coefficient ρ between the FFB obtained with the PSE criterion and the FFB obtained with the crack-growth criterion is

0.57, at a significance level p = 0.051, so about two thirds of the variance of one ranking is not explained by the other. The alternative LAS indices are not redundant with fatigue life either: over the fourteen binders, the FREI correlates only weakly with $N_{f,1.25\%}$ under the PSE criterion (ρ = 0.41). Rutting resistance and damage tolerance are, in this set of binders, essentially independent: $J_{nr3.2}$ and the FREI give ρ = -0.14, indistinguishable from zero at this sample size (p = 0.63). A binder that resists permanent deformation therefore carries no implication about how it tolerates damage, and the definition of failure, not the material alone, decides which binder is ranked first.

The two criteria answer different questions. The peak of the stored PSE marks the transition from diffuse damage to the growth of a dominant crack and is the basis of DNIT 439/2022-ME and of the FFB classes of Table 3 (Nascimento, 2019, 2020); the crack-growth criterion of Hintz and Bahia (2013) marks the onset of unstable propagation of that crack and rewards the resistance the binder retains after localisation, which the post-peak indices of Zhang et al. (2022) also describe. The RET systems rank higher under the PSE criterion because their stress decays more slowly after the peak (strain tolerance of 21.7% to 23.6% against 14.5% to 16.1% for the particle-only systems, Table 9), whereas under the crack-growth criterion the modified binders fall closer to one another and to CAP 50/70 (Table 8): once a crack dominates, the particles and the terpolymer add less resistance to its propagation than the elastomeric network of AMP 60/85-E. On the first basis the best modified binder is 3nC + RET, on the second 7nC + RET, and these two are the only modified binders in the top three under both criteria.

To make the dependence explicit, the fourteen binders were ranked with a composite score built on three families of indices. The rutting family holds $J_{nr0.1}$, $J_{nr3.2}$, $J_{nr,diff}$, and the continuous PG after the RTFO; the fatigue family holds the FFB and the fatigue life at 1.25% strain under both criteria, the FREI, the average reduction in integrity, the strain tolerance, and the strain energy tolerance; the ageing family holds the ageing index, the mass loss, the retained penetration, and the two oxidation indices. Each property was normalised between 0 and 1 by its minimum and maximum among the fourteen binders (Tables 4, 5, 7, 8, and 9), with the sign set so that a higher normalised value is always the better one and the fatigue life entering as $\log_{10} N_f$, and the score of a binder is the weighted sum of its normalised properties, the highest score taking rank 1. The weight of a family is split evenly among its members. Four weightings were applied: three that concentrate 0.60 of the weight on one family and 0.20 on each of the other two, and a balanced weighting that gives one third to each family, which represents an application where no single distress governs. Fig. 12 shows how each binder moves between the weightings.

The ranking is sensitive to the weights, and that sensitivity is the result. AMP 60/85-E moves six positions: first when fatigue dominates, seventh when rutting dominates, and seventh again when ageing dominates. Its $J_{nr,diff}$ of 48.7% is far above that of every other binder, and its ageing index (1.66) and retained penetration (73%) are worse than those of all six RET systems, whose ageing indices lie between 1.50 and 1.59 and whose retained penetrations lie between 81% and 87%. The three chemical, empirical, and rheological measurements of ageing agree on this, which is why the result does not rest on a single index. 10mC + RET is first when rutting or ageing dominates and fourth when fatigue dominates. Under the balanced weighting the leader is 7nC + RET, ahead of 10mC + RET and 10nC + RET, with AMP 60/85-E fourth: once the three distresses carry equal weight, the commercial reference no longer heads the ranking. Two formulations stand out, for different reasons. 7nC + RET takes the first position under the balanced weighting and the second under the fatigue-dominant one, behind AMP 60/85-E alone. In the baseline scheme, 10nC + RET never leaves the top three under any of the four weightings, and it is the only binder of the study of which that is true. CAP 50/70 is last under every weighting.

Because the position of a binder also depends on how the score is built, the construction was varied in ten ways: rank and z-score normalisation in place of min-max scaling, fatigue life entered linearly, equal weight per index, removal of $J_{nr,diff}$ or of the two FTIR indices, inclusion of the VAI, and three alternative compositions of the fatigue family. The structure of the ranking is stable: CAP 50/70 is last in 43 of the 44 combinations of scheme and weighting, the six RET systems rank above the six particle-only systems in all 44, and the Spearman correlation between each alternative balanced ranking and the baseline is 0.90 or higher. The identity of the leader is not: 7nC + RET is first under the balanced weighting in seven of the eleven schemes, and the balanced scores of the three leading RET formulations (0.836, 0.820, and 0.818) and of AMP 60/85-E (0.791) lie within 0.05 of one another, so the composite score separates groups of binders rather than the formulations inside the leading group.

Four qualifications bound this reading. First, the ageing family rests on short-term ageing, so the ranking describes resistance to the ageing imposed during mixing and construction rather than long-term field durability. Second, the fatigue deficit of the modified binders relative to AMP 60/85-E is real and is not resolved by any weighting: the best modified binder reaches 83% of its fatigue life under the PSE criterion and 71% under the crack-growth criterion. Third, the viscosity ageing index carries zero weight in the ageing family, for the reason given earlier; giving it weight does not change the conclusion, because AMP 60/85-E has the highest VAI of the fourteen binders and the RET systems move further ahead. Fourth, for the systems with RET the carbonyl index is not a clean measure of oxidation, since the terpolymer contributes to the same band; removing the two oxidation indices leaves 7nC + RET first under the balanced weighting. The practical reading is that the choice among the RET formulations should follow the governing distress: 10mC + RET where rutting or ageing governs; 7nC + RET where fatigue governs or where the three distresses carry equal weight; and 10nC + RET where the governing distress cannot be established in advance, since its position depends least on the weighting.

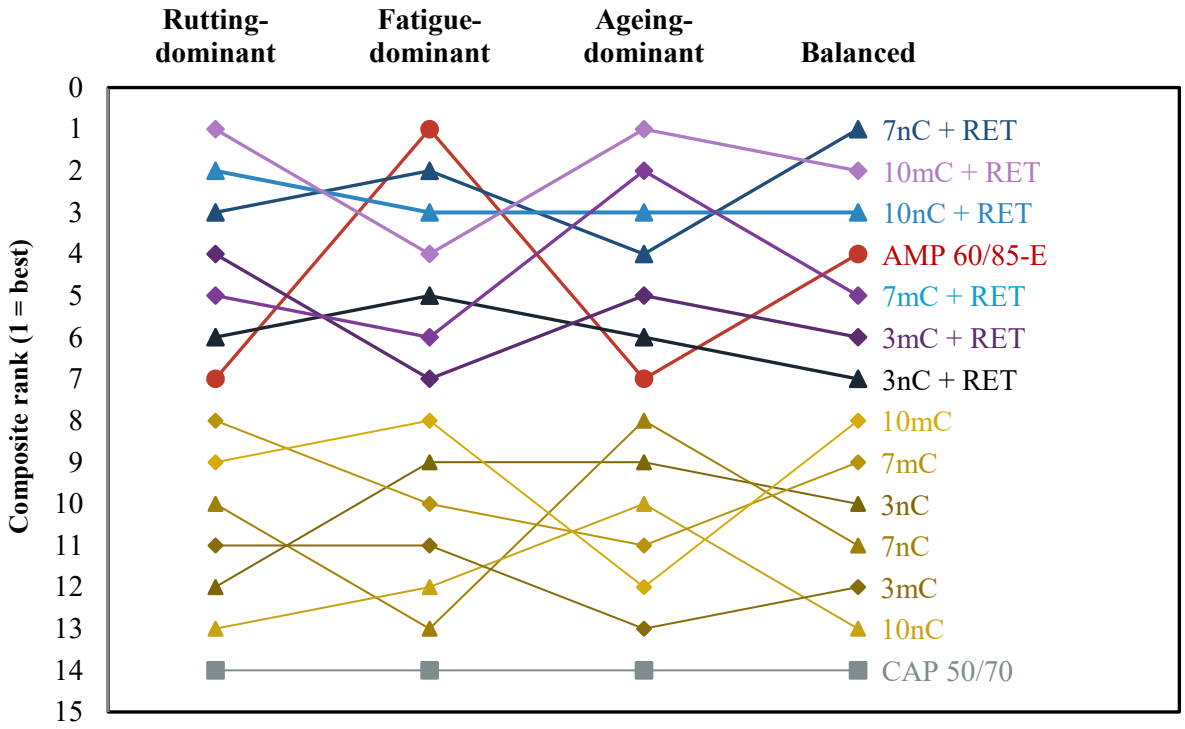


Fig. 12. Composite rank of the fourteen binders under four weightings of the performance families (weights given in the order rutting, fatigue, and ageing).

3.5. Apportioning the effects of the terpolymer and the particles

The experimental design compares each particle-modified binder with CAP 50/70 and with its terpolymer counterpart. The effect of the terpolymer is therefore measured as the effect of adding RET to a particle-modified binder, and the share of the gains attributable to each modifier is estimated from the dependence of each property on the particle content within the RET systems: the slope with content measures what the particles still do in the presence of the terpolymer, and the linear intercept at zero content estimates the response of a binder with RET alone under the assumption that the two effects are additive. Table 10 lists both quantities for the properties that carry the main conclusions, with the coefficient of determination of each three-point fit.

Three groups of properties emerge. Consistency depends on the particle content in both series: penetration falls by about 0.85 (0.1 mm) and the softening point after the RTFO rises by 0.2 °C to 0.5 °C per 1% of particles, with intercepts of 45 to 46 (0.1 mm) and 63 °C that lie far from the values of CAP 50/70 (59 and 52 °C). Rutting resistance depends on it as well: $J_{nr3.2}$ falls by 0.04 1/kPa per 1% in both series, and the intercept of about 1.35 1/kPa, inside the H class of AASHTO M 332, implies that the terpolymer alone would account for roughly 87% of the reduction from the 4.4 1/kPa of CAP 50/70 to the 0.9 1/kPa of the best formulations, and the particles for the remaining 13%. The ageing and fatigue indices depend weakly or not at all on content within the RET systems: per 1% of particles, the ageing index changes by less than 0.005, the crack-growth FFB by 0.002 or less, the strain tolerance by 0.15 percentage points or less, and the FFB under the PSE criterion by about 0.005 in the nano series and not at all in the micro series, while the mass loss varies within 0.08 percentage points without a common direction between the two series. The intercepts of these indices (ageing index 1.54, FFB under the PSE criterion 1.47 to 1.53, strain tolerance 21% to 23%) coincide with the measured RET systems and lie far from the

particle-only systems, so these responses are attributed to the terpolymer. For the ageing indices the two modifiers act in the same direction: retained penetration shows that the particles alone already carry most of the gain on that index, so the ageing family of the composite score rewards the RET systems for the combined effect of the two modifiers rather than for the terpolymer alone. The same applies to the stress sensitivity, which falls with the particle content in both series (by 1.2% to 1.9% per 1%) and whose intercept (17% to 31%) remains below the 48.7% of AMP 60/85-E.

Table 10. Linear dependence of selected properties on the particle content within the RET systems.

Property	CAP 50/70	Slope per 1% (nano series)	Intercept at 0% (nano)	r^2	Slope per 1% (micro series)	Intercept at 0% (micro)	r^2
Penetration, unaged (0.1 mm)	59	-0.85	45	0.99	-0.86	46	0.99
Softening point after RTFO (°C)	52	0.55	62.9	0.78	0.19	63.5	0.56
Continuous PG after RTFO (°C)	62.6	0.30	72.3	0.78	0.04	72.5	0.02
$J_{nr3.2}$ (1/kPa)	4.4	-0.042	1.35	0.93	-0.041	1.37	0.68
$J_{nr,diff}$ (%)	5.0	-1.86	31.1	0.98	-1.17	17.3	0.56
Retained penetration (%)	69	0.69	78.4	0.84	0.42	82.5	0.93
Ageing index AI	2.07	0.0039	1.54	0.44	-0.0019	1.54	0.10
Mass loss (%)	0.33	-0.0027	0.101	0.68	0.0108	-0.035	0.68
FFB (PSE)	1.34	-0.0045	1.53	0.82	0.0000	1.47	n/a
$\log_{10} N_{f,1.25\%}$ (PSE)	4.83	-0.0137	5.51	0.80	-0.0037	5.33	0.99
FFB (crack growth)	1.24	-0.0020	1.29	0.04	-0.0015	1.27	0.82
ε_T (%)	15.7	-0.066	23.4	0.07	0.152	21.3	1.00
FREI	1.12	-0.0041	0.92	0.00	-0.0312	1.17	0.41

r^2 = coefficient of determination of the three-point fit (n/a when the three values coincide). Intercepts are extrapolations to zero particle content that assume additive effects of the terpolymer and the particles. Penetration before ageing; all other properties after the RTFO.

3.6. Scope and limitations

The findings are bounded by five features of the experimental programme. First, the attribution of effects to the terpolymer rests on paired comparisons and on the extrapolation of Table 10, which assumes additivity; a binder with the terpolymer alone would quantify the interaction between the two modifiers. Second, the particles were characterised in the dry state, and the hypotheses of agglomeration and of a particle network were examined through the linear viscoelastic master curves and the LAS indices; direct observation of the particles inside the binder would complete the picture of the loss of fatigue efficiency at high nanoparticle contents. Third, the micro and nano products differ in agglomerate morphology and, in all likelihood, in specific surface area, so the micro/nano comparison is a comparison between two commercial products rather than a pure size effect.

Fourth, ageing was simulated with the RTFO, so the ageing family of the composite score, the fatigue results, and the ranking describe the state of the binders after mixing and construction; long-term ageing in the pressure ageing vessel is the natural extension, since polymer-modified and particle-modified systems can age differently in service. Fifth, the results are binder-scale. The transfer of binder performance to the mixture is mediated by the aggregate skeleton, the film thickness, and the interaction with the mineral filler, and the correlation between binder and mixture fatigue is itself imperfect (Bessa et al., 2019; Osmari et al., 2023; Enríquez-León et al., 2025); mixture tests of permanent deformation and fatigue are the next step before a field recommendation. The work was conducted on a single base binder and at a single terpolymer content, and extrapolation to other binders and dosages requires confirmation.

4. Conclusions

This research evaluated the incorporation of calcium carbonate micro- and nanoparticles, alone and combined with the reactive terpolymer RET, and its effects on the empirical, chemical, and rheological properties of a CAP 50/70 asphalt binder. Based on the tests performed and the analysis of the results, the following conclusions were drawn.

The FTIR analysis indicated that the reactive terpolymer formed ester and ether bonds with the asphalt matrix, consistent with effective compatibilisation, whereas the particles alone acted through physical interactions; the intensification of the carbonate bands confirmed their incorporation into the binder.

Under short-term ageing, the nanoparticle-modified binders, especially when combined with RET, performed better than CAP 50/70 on the ageing index and the retained penetration, and some RET systems matched or exceeded AMP 60/85-E; on retained penetration, the particles alone already provide most of the gain.

All modified binders reached longer fatigue lives than CAP 50/70 under the PSE criterion, and the terpolymer systems stood out for their post-peak strain tolerance. The content that optimises fatigue depends on the failure criterion (3% of nanoparticles under the PSE criterion, 7% with RET under the crack-growth criterion) and is not the content that optimises permanent deformation.

The comparison between micro- and nanoparticles does not support the claim that reducing the particle size was decisive: the nano systems lead the fatigue life under the PSE criterion in four of the six paired formulations, but the micro systems lead the crack-growth FFB and the FREI in most pairs, and 10mC outperforms 10nC in $J_{nr3.2}$. The advantage of the nanoscale is restricted to specific indices and is clearest at 3%, and the two products differ in agglomeration state, so the comparison is between two commercial products rather than a pure size effect.

For permanent deformation, the particles improve consistency and flow resistance, with the best results at 10% for the microparticles and 7% for the nanoparticles among the particle-only systems, and at 10% for both once RET is present. Adding the terpolymer produced the largest gains in both distresses; a linear extrapolation within the RET series attributes about 87% of the reduction in $J_{nr3.2}$ to the terpolymer. The combination produced binders that approach, and in specific responses exceed, the high-performance reference AMP 60/85-E.

Weighing the three distress families together supports this reading: RET formulations with 10% particles led when rutting carried the greatest weight, the six RET systems placed ahead of AMP 60/85-E when short-term ageing did, and 7nC + RET came first under equal weights, with AMP 60/85-E fourth. The commercial reference kept the first position whenever fatigue dominated. The ordering of the groups held under ten alternative constructions of the score, the identity of the leader did not, and 10nC + RET was the formulation whose standing depended least on the weighting.

The conclusions apply to short-term aged binders, at the laboratory scale and on a single base binder, and attribute effects to the terpolymer through paired comparisons and an additive extrapolation. Future work should add a CAP 50/70 with 1.8% RET and no particles, characterise the particles inside the binder, add long-term ageing, extend the evaluation to asphalt mixtures, and assess the cost of the combined modification.

Declaration of generative AI use

The authors used a generative AI tool (Claude, Anthropic) to assist with editing the manuscript text. All data, analyses, and interpretations were produced and verified by the authors, who take full responsibility for the content of the manuscript.

References

Agência Nacional do Petróleo, Gás Natural e Biocombustíveis. (2022). Resolução ANP nº 897/2022: Regulamento técnico de cimentos asfálticos de petróleo. Brasília: ANP. [In Portuguese]

Airey, G. D. (2003). Rheological properties of styrene butadiene styrene polymer modified road bitumens. Fuel, 82(14), 1709-1719.

Alamnie, M. M., Taddesse, E., & Hoff, I. (2023). A study on permanent deformation and fatigue damage interaction in asphalt concrete. Construction and Building Materials, 407, 133473.

Alas, M., Abba, S. I., Ali, S. I. A., Rahim, A., & Yusoff, N. I. M. (2022). Evaluating the performance of aluminum oxide nanoparticle-modified asphalt binder and modelling the viscoelastic properties by using artificial neural networks and support vector machines. Advances in Materials Science and Engineering, 2022, 9685454.

Albayati, A. H., Al-Ani, A. F., Byzyka, J., Al-Kheetan, M., & Rahman, M. (2024). Enhancing asphalt performance and its long-term sustainability with nano calcium carbonate and nano hydrated lime. Sustainability, 16(4), 1507.

American Association of State Highway and Transportation Officials. (2021). AASHTO M 332: Standard specification for performance-graded asphalt binder using multiple stress creep recovery (MSCR) test. Washington, DC: AASHTO.

American Association of State Highway and Transportation Officials. (2019). AASHTO T 315: Standard method of test for determining the rheological properties of asphalt binder using a dynamic shear rheometer (DSR). Washington, DC: AASHTO.

Anupam, B. R., Sahoo, U. C., & Chandrappa, A. K. (2022). A methodological review on self-healing asphalt pavements. Construction and Building Materials, 321, 126395.

Ashish, P. K., & Singh, D. (2019). Use of nanomaterial for asphalt binder and mixtures: A comprehensive review on development, prospect, and challenges. Road Materials and Pavement Design.

Associação Brasileira de Normas Técnicas. (2006). NBR 15086: Materiais betuminosos - Determinação da recuperação elástica pelo ductilômetro de cimentos asfálticos modificados por polímeros elastoméricos ou borracha. Rio de Janeiro: ABNT. [In Portuguese]

Associação Brasileira de Normas Técnicas. (2007). NBR 6576: Materiais asfálticos - Determinação da penetração. Rio de Janeiro: ABNT. [In Portuguese]

Associação Brasileira de Normas Técnicas. (2012). NBR 6296: Produtos betuminosos semissólidos - Determinação da massa específica e densidade relativa. Rio de Janeiro: ABNT. [In Portuguese]

Associação Brasileira de Normas Técnicas. (2016). NBR 6560: Ligantes asfálticos - Determinação do ponto de amolecimento - Método do anel e bola. Rio de Janeiro: ABNT. [In Portuguese]

Associação Brasileira de Normas Técnicas. (2021). NBR 15184: Materiais betuminosos - Determinação da viscosidade em temperaturas elevadas usando um viscosímetro rotacional. Rio de Janeiro: ABNT. [In Portuguese]

ASTM International. (2019). ASTM D2872: Standard test method for effect of heat and air on a moving film of asphalt (rolling thin-film oven test). West Conshohocken, PA: ASTM International.

ASTM International. (2020). ASTM D5M: Standard test method for penetration of bituminous materials. West Conshohocken, PA: ASTM International.

ASTM International. (2020). ASTM D36M-14: Standard test method for softening point of bitumen (ring-and-ball apparatus). West Conshohocken, PA: ASTM International.

ASTM International. (2020). ASTM D7173-20: Standard practice for determining the separation tendency of polymer from polymer-modified asphalt. West Conshohocken, PA: ASTM International.

ASTM International. (2020). ASTM D7405: Standard test method for multiple stress creep and recovery (MSCR) of asphalt binder using a dynamic shear rheometer. West Conshohocken, PA: ASTM International.

ASTM International. (2021). ASTM D6373: Standard specification for performance-graded asphalt binder. West Conshohocken, PA: ASTM International.

Azahar, W. N. A. W., Bujang, M., Ramadhansyah, P. J., Hainin, M. R., Aziz, M. M. A., & Ngadi, N. (2015). Application of nanotechnology in asphalt binder: A conspectus and overview. Jurnal Teknologi (Sciences & Engineering), 76(14), 85-89.

Bessa, I. S., Vasconcelos, K. L., Castelo Branco, V. T., & Bernucci, L. L. (2019). Fatigue resistance of asphalt binders and the correlation with asphalt mixture behaviour. Road Materials and Pavement Design, 20(sup2), S695-S709.

Business Research Insights. (2024). SBS modified asphalt market: Global industry analysis and forecast.

Cheng, G., Zheng, Y., Yu, J., et al. (2022). Investigation of the fatigue life of bottom-up cracking in asphalt concrete pavements. Applied Sciences, 12(23), 12119.

Departamento Nacional de Infraestrutura de Transportes. (2006). DNIT 095/2006-EM: Cimentos asfálticos de petróleo - Especificação de material. Rio de Janeiro: IPR. [In Portuguese]

Departamento Nacional de Infraestrutura de Transportes. (2010). DNIT 130/2010-ME: Determinação da recuperação elástica de materiais asfálticos pelo ductilômetro - Método de ensaio. Rio de Janeiro: IPR. [In Portuguese]

Departamento Nacional de Infraestrutura de Transportes. (2020). DNIT 423/2020-ME: Pavimentação - Ligante asfáltico - Fluência e recuperação de ligante asfáltico determinados sob tensões múltiplas (MSCR) - Método de ensaio. Rio de Janeiro: IPR. [In Portuguese]

Departamento Nacional de Infraestrutura de Transportes. (2022). DNIT 439/2022-ME: Pavimentação - Ligante asfáltico - Avaliação da resistência à fadiga de ligantes asfálticos usando varredura de amplitude linear (LAS) - Método de ensaio. Rio de Janeiro: IPR. [In Portuguese]

Duarte, E. V. N., Rodrigues, J. K. G., Mendonça, A. M. G. D., Melo Neto, O. M., Costa, D. B., & Lima, R. K. B. (2023). Rheological properties of asphalt binder modified with reactive/non-reactive polymer and polyphosphoric acid. Transportation Research Record, 2677(3), 1567-1578.

Enríquez-León, A. J., Rocha, M. L., Osmari, P. H., Leite, L. F. M., de Barros, L. M., Aragão, F. T. S., & do Nascimento, L. A. H. (2025). Component-based damage characterization of asphalt mixtures considering binder rheological indexes and aggregate morphology. Construction and Building Materials, 466, 140199.

Gama, D. A. (2016). Efeito da adição de polímeros reativo, não-reativo e ácido polifosfórico e suas combinações nas propriedades de ligantes asfálticos (Doctoral thesis). Universidade Federal de Campina Grande, Campina Grande. [In Portuguese]

García Mainieri, J. J., Singhvi, P., Ozer, H., Sharma, B. K., & Al-Qadi, I. L. (2021). Fatigue tolerance of aged asphalt binders modified with softeners. Transportation Research Record, 2675(11), 1229-1244.

Gulzar, S., Xue, L., Preciado, J., Fried, A., Castorena, C., Underwood, B. S., Habbouche, J., & Boz, I. (2024). Phenomenological modeling of aging and rejuvenation on asphalt binder fatigue characteristics. Construction and Building Materials, 425, 135929.

Hamedi, G. H., Pirbasti, M. H., & Pirbasti, Z. R. (2023). Investigating the effect of using waste ultrahigh-molecular-weight polyethylene on the fatigue life of asphalt mixture. Periodica Polytechnica Civil Engineering, 64(4).

He, H., Zhang, Z., Wang, J., & Li, K. (2013). Compressive properties of nano-calcium carbonate/epoxy and its fibre composites. Composites Part B: Engineering, 45(1), 919-924.

He, Y., Zeng, Q., Liu, Y., Liu, P., Zeng, Y., Xu, Z., & Liu, Q. (2021). Evaluation of the composite mechanism of nano-Fe2O3/asphalt based on molecular simulation and experiments. Materials, 14, 3425.

Hintz, C., & Bahia, H. (2013). Simplification of linear amplitude sweep test and specification parameter. Transportation Research Record, 2370(1), 10-16.

Lesueur, D. (2009). The colloidal structure of bitumen: Consequences on the rheology and on the mechanisms of bitumen modification. Advances in Colloid and Interface Science, 145(1-2), 42-82.

Lu, D. X., Bui, H. H., & Saleh, M. (2024). Predicting the rutting behaviour of asphalt concrete in the modified wheel tracking test using DEM and a cohesive viscoelastic-elastoplastic-damage contact model. Computational Particle Mechanics, 11, 2819-2837.

Lu, X., & Isacsson, U. (2002). Effect of ageing on bitumen chemistry and rheology. Construction and Building Materials, 16(1), 15-22.

Manfro, A. L., Staub de Melo, J. V., Villena Del Carpio, J. A., & Broering, W. B. (2022). Permanent deformation performance under moisture effect of an asphalt mixture modified by calcium carbonate nanoparticles. Construction and Building Materials, 342, 128087.

Marinho Filho, P. G. T., dos Santos, A. T. R., Lucena, L. C. F. L., & Tenório, E. A. G. (2020). Rheological evaluation of asphalt binder modified with nanoparticles of titanium dioxide. International Journal of Civil Engineering, 18(10), 1195-1207.

Martins, A. T. (2014). Contribuição para a validação do ensaio de resistência ao dano por fadiga para ligantes asfálticos (Master dissertation). Universidade Federal do Rio de Janeiro, Rio de Janeiro. [In Portuguese]

Staub de Melo, J. V., Manfro, A. L., Barra, B. S., Dell'Antonio Cadorin, N., & Borba Broering, W. (2023). Evaluation of the rheological behavior and the development of performance equations of asphalt composites produced with titanium dioxide and zinc oxide nanoparticles. Nanomaterials, 13, 288.

Melo Neto, O. M., Ferreiro, A. A., Freire, T. S., Silva, G. C. B., Lucena, L. C. F. L., & Sousa Neto, V. F. (2020). Rheological analysis of asphalt binders modified with hydrated lime and titanium dioxide nanoparticles. International Journal for Innovation Education and Research, 8(11), 579.

Nascimento, L. A. H. (2019). Seleção de ligantes e misturas asfálticas (Internal report CENPES/PETROBRAS RT PROD 007/2019). [In Portuguese]

Nascimento, L. A. H. (2020). Consolidação de novas técnicas para avaliação de materiais asfálticos (Internal report CENPES/PETROBRAS RT PROD 005/2020). [In Portuguese]

Oliveira, Y. M. M. (2022). Reologia de ligantes asfálticos e suas variações frente à incorporação de polímeros e ao envelhecimento simplificado como RTFOT (Master dissertation). Universidade Federal de Santa Catarina, Florianópolis. [In Portuguese]

Osmari, P. H., Leite, L. F. M., do Nascimento, L. A. H., Espíndola, R. P., & Aragão, F. T. S. (2023). Characterization of the fatigue behavior of asphalt binders, FAMs, and AC mixtures based on multiscale approaches and the S-VECD model. Construction and Building Materials, 394, 132165.

Possebon, É. P. (2021). Caracterização avançada de ligantes e misturas asfálticas brasileiras (Doctoral thesis). Universidade Federal de Santa Maria, Santa Maria. [In Portuguese]

Queiroz, R. F. R. (2022). Avaliação do dano por fadiga de misturas asfálticas modificadas por adição de polímero a partir do modelo S-VECD (Master dissertation). Universidade Federal de Campina Grande, Campina Grande. [In Portuguese]

Rahim, A., El Badawy, A., & Cox, T. (2024). Surface-modified nanoclays for enhancing resistance to moisture damage in hot mix asphalt. American Journal of Civil Engineering, 12(3), 76-85.

Ramadhansyah, P. J., Masri, K. A., Norhidayah, A. H., Hainin, M. R., Naqiuddin, M. W., Haryati, Y., Satar, M. K. I. M., & Juraidah, A. (2020). Nanoparticle in asphalt binder: A state-of-the-art review. IOP Conference Series: Materials Science and Engineering, 712, 012023.

Rocha, M. L., Enríquez-León, A. J., Aragão, F. T. S., Espíndola, R. P., & do Nascimento, L. A. H. (2024). Exploring the effects of volumetrics and binder properties on the performance of asphalt mixtures. Construction and Building Materials, 438, 137054.

Santos, K. P., Lucena, A. E. F. L., Lucena, L. C. F. L., Silva, J. A. A., & Costa, S. C. F. E. (2015). Estudo da incorporação de argilas montmorilonitas em cimentos asfálticos de petróleo. Revista Matéria, 20(2), 501-513. [In Portuguese]

Sargheini, J., Ataie, A., Salili, S. M., & Hoseinion, A. A. (2012). One-step facile synthesis of CaCO3 nanoparticles via mechano-chemical route. Powder Technology, 219, 72-77.

Sousa Neto, V. F., Lucena, L. C. F. L., Barros, A. G., Lucena, A. E. F. L., & Marinho Filho, P. G. T. (2022). Rheological evaluation of asphalt binder modified with zinc oxide nanoparticles. Case Studies in Construction Materials, 17, e01224.

Sousa Neto, V. F., Minervina Silva, I., Lucena, L. C. F. L., Lucena, A. E. F. L., Melo Neto, O. M., & Lima, R. K. B. (2023). Effect of superficially modified zinc oxide nanoparticles as an additive on the rheological performance of asphalt binder. Road Materials and Pavement Design, 25(6), 1211-1228.

Sun, Z., Yi, J., Huang, Y., Feng, D., & Guo, C. (2016). Properties of asphalt binder modified by bio-oil derived from waste cooking oil. Construction and Building Materials, 102, 496-504.

Tsuzuki, T., & McCormick, P. G. (2004). Mechanochemical synthesis of nanoparticles. Journal of Materials Science, 39, 5143-5146.

Wang, R., Yue, M., Xiong, Y., & Yue, J. (2021). Experimental study on mechanism, aging, rheology and fatigue performance of carbon nanomaterial/SBS-modified asphalt binders. Construction and Building Materials.

Xu, S., García, A., Su, J., Liu, Q., Tabakovic, A., & Schlangen, E. (2018). Self-healing asphalt review: From idea to practice. Advanced Materials Interfaces.

Yang, S., Park, H., & Baek, C. (2023). Fatigue cracking characteristics of asphalt pavement structure under aging and moisture damage. Sustainability, 15(6), 4815.

Yao, H., You, Z., Li, L., Lee, C. H., Wingard, D., Yap, Y. K., & Shi, X. (2013). Properties and chemical bonding of asphalt and asphalt mixtures modified with nanosilica. Journal of Materials in Civil Engineering.

Yu, X., Li, D., Leng, Z., Yao, H., & Wang, S. (2023). Weathering characteristics of asphalt modified by hybrid of micro-nano tire rubber and SBS. Construction and Building Materials, 389, 131785.

Zhang, D., Chen, Z., Zhang, H., & Wei, C. (2018). Rheological and anti-aging performance of SBS modified asphalt binders with different multi-dimensional nanomaterials. Construction and Building Materials, 188, 409-416.

Zhang, H., Zhu, C., Yu, J., Shi, C., & Zhang, D. (2015). Influence of surface modification on physical and ultraviolet aging resistance of bitumen containing inorganic nanoparticles. Construction and Building Materials, 98, 735-740.

Zhang, Y. (2019). Investigation on preparation process and storage stability of modified asphalt binder by grafting activated crumb rubber. Materials, 12(12), 2014.

Zhang, L., Gao, X., Wang, W., Wang, H., & Zheng, K. (2021). Laboratory evaluation of rheological properties of asphalt binder modified by nano-TiO2/CaCO3. Advances in Materials Science and Engineering, 2021, 5522025.

Zhang, R., Sias, J. E., & Dave, E. V. (2022). Development of new performance indices to evaluate the fatigue properties of asphalt binders with ageing. Road Materials and Pavement Design, 23(2), 377-396.

Zhao, Z., Wu, S., Liu, Q., Yang, C., Zou, Y., & Wan, P. (2022). Feasibility assessment of CeO2 nanoparticles as aging-resistant agent of asphalt. Construction and Building Materials, 330, 127245.

Zhou, F., Karki, P., & Im, S. (2017). Development of a simple fatigue cracking test for asphalt binders. Transportation Research Record, 2632(1), 79-87.

Zhou, T., Wan, S., Dong, Z., Xie, S., You, L., & Jin, C. (2026). Physicochemical mechanisms of asphalt-aggregate interface adhesion: Effects of mineral composition and surface energy. Construction and Building Materials, 513, 145469.